Review Article

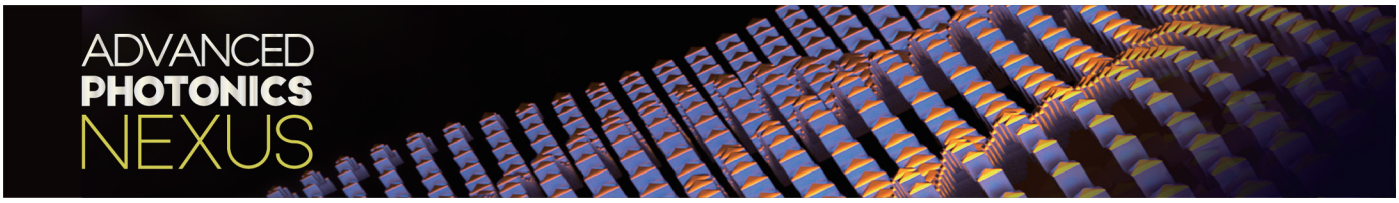

Evolution on spatial patterns of structured laser beams: from spontaneous organization to multiple transformations

Xin Wang,[a,b,c,†] Zilong Zhang,[a,b,c,*,†] Xing Fu,[d,e] Adnan Khan,[f] Suyi Zhao,[a,b,c] Yuan Gao,[a,b,c] Yuchen Jie,[a,b,c] Wei He,[a,b,c] Xiaotian Li,[a,b,c] Qiang Liu,[d,e,*] and Changming Zhao[a,b,c]

[a]Beijing Institute of Technology, School of Optics and Photonics, Beijing, China
[b]Ministry of Education, Key Laboratory of Photoelectronic Imaging Technology and System, Beijing, China
[c]Ministry of Industry and Information Technology, Key Laboratory of Photonics Information Technology, Beijing, China
[d]Tsinghua University, Ministry of Education, Key Laboratory of Photonic Control Technology, Beijing, China
[e]Tsinghua University, State Key Laboratory of Precision Measurement Technology and Instruments, Department of Precision Instrument, Beijing, China
[f]Nankai University, School of Physics, Key Laboratory of Weak Light Nonlinear Photonics, Tianjin, China

Abstract. Spatial patterns are a significant characteristic of lasers. The knowledge of spatial patterns of structured laser beams is rapidly expanding, along with the progress of studies on laser physics and technology. Particularly in the last decades, owing to the in-depth attention on structured light with multiple degrees of freedom, the research on spatial and spatiotemporal structures of laser beams has been promptly developed. Such beams have hatched various breakthroughs in many fields, including imaging, microscopy, metrology, communication, optical trapping, and quantum information processing. Here, we would like to provide an overview of the extensive research on several areas relevant to spatial patterns of structured laser beams, from spontaneous organization to multiple transformations. These include the early theory of beam pattern formation based on the Maxwell–Bloch equations, the recent eigenmodes superposition theory based on the time-averaged Helmholtz equations, the beam patterns extension of ultrafast lasers to the spatiotemporal beam structures, and the structural transformations in the nonlinear frequency conversion process of structured beams.

Keywords: spatial patterns; transverse modes; spatiotemporal beams; structured laser beams; nonlinear optics.

Received Oct. 11, 2022; accepted for publication Jan. 6, 2023; published online Feb. 6, 2023.

[DOI: 10.1117/1.APN.2.2.024001]

1 Introduction

Since their introduction 60 years ago,[1] lasers with various characteristics have developed rapidly, making them important light sources in various fields ranging from scientific research[2–4] to industrial production.[5–8] Almost all the characteristics of a laser can be classified as temporal,[9–14] spatial,[15–18] or spectral domain.[19–23] Over the past few decades, much interest has been given to laser properties in the temporal and spectral domains, while the spatial properties of laser beams seem to be relatively less emphasized. In the last 10 to 20 years, as a result of the emergence of research on spatial characteristics of laser beams, especially, the orbital angular momentum (OAM), much more attention has been paid to structured laser beams with distinct spatial or spatiotemporal structures. Such beams have brought various breakthroughs to many fields, including imaging,[24,25] microscopy,[26,27] metrology,[28–30] communication,[31–33] optical trapping,[34–36] and quantum information processing.[37–39] In the most recent five years, the number of reviews on structured light has boomed, with the majority of reviews focusing on technical-level research into the phenomenon,[40–54] such as the generation and detection technology of structured light,[44,45] application in the field of optical trapping[46,47] and anti-turbulence,[48] progress in optical vortices[49–51] and higher-dimensional structured light,[52]

*Address all correspondence to Zilong Zhang, zlzhang@bit.edu.cn; Qiang Liu, qiangliu@tsinghua.edu.cn

†These authors contributed equally to this work.

as well as research on structured light in flat optics[53] and nonlinear optics.[54] In contrast, there have been few studies on the evolution of the investigations and corresponding understandings of the pattern formation of structured laser beams. Here, we would like to take the spatial patterns as the main core to review the evolution and recent advancement on spatial patterns of structured laser beams, from the early spontaneous organization with numerical solutions of mathematical equations and eigenmode superposition theories to the multiple transformations of the spatiotemporal dimensions and nonlinear process of structured laser beams.

The research on spatial patterns of structured laser beams went through two periods: the first was the spontaneous organization of patterns described by relative equations, while the second was the transformation of laser patterns on demand. Although there is no distinct separation between these two periods, it is noticeable that over the past 10 years, we have steadily gained a better understanding of how diverse laser spatial patterns originate and developed several effective techniques for producing spatial patterns on demand. Research on the formation of structured laser patterns was a main focus in physics from the 1960s to 1990s.[55–69] The earliest research at that time combined Maxwell's equations[69] with Schrödinger's equation,[70] leading to the laser amplitude E coupled with the collective variables P and D for the atomic polarization and population inversion to describe the transverse mode formation.[71] This set of equations is called the MB equations.[62,72] Then, on the basis of the MB equations, which are a set of spatiotemporal multivariate nonlinear partial differential equations, the pattern formation characteristics of class A, B, and C lasers were successively studied.[68,71] The relevant equations are then further developed, and equations, such as the complex Ginzburg–Landau (CGL),[73,74] complex Swift–Hohenberg (CSH),[75,76] and Kuramoto–Sivashinsky (KS)[77–80] equations were further derived. Through the numerical solution of these equations, the formation of laser transverse patterns under specific parameters can be analyzed. In addition, with time and space terms involved, these equations can explain both the spatial and temporal characteristics of the patterns in some cases, including stability, oscillation, chaos, and so on.[81–83] However, most of these patterns are ideal cases obtained under the condition of a single transverse mode of the laser.[62] If multiple transverse modes with different frequencies are involved, it would be hard to analyze the results of multifrequency interaction through these equations. Therefore, in the study of pattern formation in the last 20 years, the analysis is often carried out through the applications of a set of eigenmode superposition theories.[84–89] This set of theories mainly studies the spatial structure characteristics of the patterns. The basis of eigenmode superposition theory is the fundamental composed modes, such as Hermite–Gaussian (HG), Laguerre–Gaussian (LG), and Ince–Gaussian (IG) modes, obtained by solving the Helmholtz equations,[90–96] except with space terms and without time terms. Then, according to the specific laser cavity conditions and field distributions of the output pattern, it could be analyzed whether coherent or incoherent superposition of the fundamental modes is generated through the eigenmode superposition theory. This involves the concept of transverse mode locking (TML),[97–99] namely, to lock the phase[100,101] or frequency of several transverse modes to obtain the output beam. The cooperatively frequency-locked multimode regime, in which at least two transverse modes contribute significantly to the output field, lock to a common frequency with which they oscillate in a synchronized way. The locking concerns also the relative phases of the modes, so that the output intensity has a stationary transverse configuration. The patterns formed by the TML effect could possess phase singularities in dark points.[102] The theory of eigenmode superposition can also explain the formation of high-order complex transverse modes and optical vortex lattices (OVLs).[87–89]

For the second period of on-demand transformation of laser patterns, a number of techniques have been developed in the past 20 years to actively control the generation and transformation of laser beam patterns, giving rise to a better understanding of the spatial features of lasers. Numerous review articles on the actively controlled generation of structured laser patterns, using both intracavity oscillation[40,41] and extracavity spatial modulation methods, are readily available.[42–45] The studies on the transformations of structured laser beams are mostly under the premise of single longitudinal mode. However, if multiple longitudinal modes are involved, the time dimension is supposed to be reconsidered. Recently, research on spatiotemporal beams has sprung up.[103–114] The direct generation of spatiotemporal beams involves the principle of spatiotemporal mode locking, i.e., locking the laser longitudinal and transverse modes at the same time to form ultrashort pulses with special spatial intensity distribution.[103] Spatiotemporal mode locking is often obtained in fiber lasers, which realizes TML with the help of spatial filtering,[107,115] and longitudinal mode locking with the help of normal-dispersion mode-locking principle[116,117] and a saturable absorber. The spatiotemporal mode-locking beam opens up a new direction for the propagation and application of nonlinear waves. However, the spatiotemporal mode-locking beams produced directly by fiber lasers often have irregular intensity distributions. To obtain regular and more complex spatiotemporal beams, a pulse shaper based on spatial light modulator (SLM) is applied, which can generate specific spatiotemporal optical vortices,[118–120] spatiotemporal Airy beams,[121] spatiotemporal Bessel beams,[122] and so on.[123–126] Another method for actively controlling the generation and transformation of structured laser beams is using nonlinear processes. Combining nonlinear frequency conversion with the generation of structured laser beams, the beam patterns of harmonic waves are found to be endowed with much richer spatial information. Through nonlinear frequency conversion of structured laser beams, the beam pattern transformations in sum frequency generation (SFG),[127–130] second-harmonic generation (SHG),[131–140] four-wave mixing (FWM),[141,142] and other frequency upconversion[143–145] processes are carried out. Usually, these studies first generate structured beams with the help of modulation devices (such as SLM), and then carry out nonlinear conversion, which belongs to the external cavity nonlinear process of structured laser beams. Meanwhile, for the intracavity nonlinear process of structured laser beams, some studies also showed similar properties, while more complex and diverse beam patterns can be obtained.[146–150]

The timeline of the evolution on spatial patterns of structured laser beams is shown in Fig. 1. In this review, we highlight the developments in laser spatial pattern studies with the emphasis on the spontaneous organization of pattern formation and the multiple transformations of laser spatial patterns. The original descriptive equations in the field of pattern formation are introduced in Sec. 2, including MB, CGL, CSH, and KS equations, which are fundamental to understanding the dynamics of pattern formation. Then, the current theories in the past 20 years are

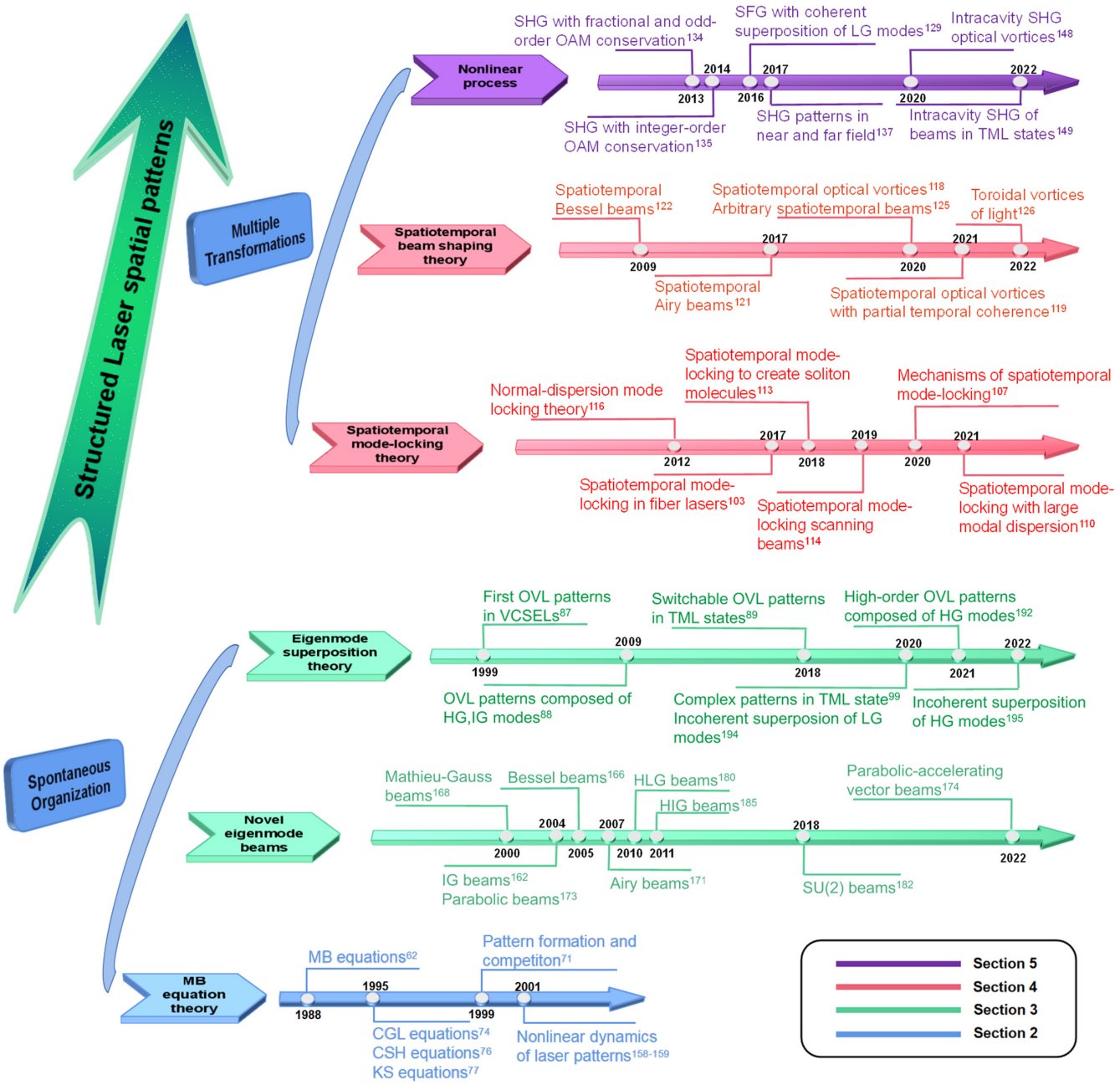

Fig. 1 Timeline of the evolution on spatial patterns of structured laser beams.

further discussed in Sec. 3, namely, the eigenmode superposition theories. The superposition of transverse modes brings a new vision in understanding laser physics and recognizing the vast possibilities for structured laser beam patterns. Results are analyzed and compared, covering coherent superpositions and incoherent superpositions. Then, in Sec. 4, more potential developments are forecast in spatiotemporal laser beams, particularly in spatiotemporal mode locking in fiber lasers and spatiotemporal beams generated through pulse shapers based on SLM. In Sec. 5, various nonlinear processes of structured laser beams from external–cavity modulations to intracavity transformation are comprehensively reviewed. Finally, concluding remarks and prospects are provided in Sec. 6.

2 MB Equations-Based Pattern Formation

Pattern formation is a ubiquitous phenomenon in nature and a phenomenon often found in laboratories; it was regarded as the spontaneous appearance of spatial order.[150] Generally, all the patterns have something in common: they appear in spatially expanding dissipative systems, which are far from equilibrium because of some external pressure. In optical systems, the mechanism of pattern formation is the interaction among diffraction, partial resonance excitation, and nonlinearity. Diffraction is responsible for spatial coupling, which is necessary for the existence of nonuniform distribution of light fields. The role of nonlinearity is to select a specific pattern from

several possible patterns. After reducing a specific model into a simpler model, a common theoretical model describing pattern formation is found to be the order parametric equation (OPE).[150,151] Then, in the study of pattern formation in structured laser systems, the problem was precisely addressed through the description of optical resonators by OPE, which reflects the general characteristics of laser transverse patterns.

The exploration of the OPE of laser spatial pattern formation can be traced back to the 1970s.[55–57] By simplifying the laser equations for the class A case to the CGL equation, the relationship between superfluid and laser dynamics was established. In view of this common theoretical description, it was expected that the dynamics of pattern formation in lasers and the dynamics of superfluidity would show identical features.[53] Then, in the late 1980s[57–60] and 1990s,[61–64,66] the formation of optical transverse modes began to be an interesting topic for scientists in MB equation field theory.

It was found that if the Maxwell equations[69] and the Schrödinger equation[70] are coupled to constrain the N atoms in the cavity and expand the field in the cavity mode, then the amplitude E is coupled with atomic polarization P and population D.[71] The set of equations is called the MB equation system, which is also the earliest manifestation of passive systems.[152] When extended to the laser system, the dynamic of the electromagnetic field in the cavity with a planar end mirror should be considered, and the planar end mirror accommodates two-energy-level atoms as an active medium. The form of the MB equation becomes[62]

$$\begin{cases} \frac{\partial E}{\partial t} = -(i\omega_c + \kappa)E + \kappa P + id\kappa\nabla^2 E \\ \frac{\partial P}{\partial t} = -\gamma_\perp P + \gamma_\perp E D \\ \frac{\partial D}{\partial t} = -\gamma_\prod\left[(D - D_0) + \frac{1}{2}(E^* P + P^* E)\right] \end{cases}, \tag{1}$$

where E is the field amplitude; P is the atomic polarization intensity; D is the population intensity; κ, $\gamma_\perp$, and $\gamma_\prod$ are the corresponding relaxation rates; ω_c is the cavity resonance frequency; and d is the diffraction coefficient. The system of Eq. (1) determines the behavior of the restricted electromagnetic field E in the transverse plane, which explains the formation mechanism of the transverse mode at the atomic level. Here, (x, y) is a plane perpendicular to the z axis of the cavity, and it is assumed that E and P have the best plane wave dependence in the z direction and the slow residual dependence on the lateral variables x and y. They directly follow the Maxwell equations of the field E together with the Bloch equations of complex atomic polarization P and population N. Numerically solving the MB equations, the laser transverse patterns observed in solid-state lasers are shown in Figs. 2(a) and 2(b).

By observing the form of the MB Eq. (1), it can be found that they are similar to the Lorentz model describing hydrodynamic instability.[154] The similarity between the Lorentz model and the MB equations implies that chaotic instability can happen in single-mode and homogeneous line lasers. However, the consideration of time scale excludes the complete dynamics of Eq. (1) in lasers. In the Lorentz model, the damping rates differ by 1 order of magnitude from each other. On the contrary, in most lasers, the three damping rates of the MB equations are different from each other. Then, according to the relationship among the three damping rates κ, $\gamma_\perp$, and $\gamma_\prod$, the MB equations can be transformed into different forms under specific laser conditions, which can describe both pattern formation and time-domain properties.[71]

For class A lasers (e.g., He–Ne, Ar, Kr, and dye): $\gamma_\perp \approx \gamma_\prod \gg \kappa$, the polarization and the population inversion of the atom can be adiabatically eliminated; hence the system is only described by one field equation. The equation can be simplified to the CGL equation, which is also the governing equation in superconductors and superfluids. Therefore, the last two equations of Eq. (1) are eliminated, leaving only the nonlinear equation representing the field amplitude E as follows:[74]

$$\frac{\partial E}{\partial \tau} = (D_0 - 1)E - i(\beta - d\nabla^2)E - g(\beta - d\nabla^2)^2 E - E|E|^2, \tag{2}$$

where τ is the scaled time. Equation (2) retains all the ingredients of spatial pattern formation in lasers. One important property of the radiation in lasers is its diffraction, which is explained by the second term on the right-hand side of Eq. (2). The third term on the right-hand side of Eq. (2) describes the spatial frequency (transverse mode) selection, a phenomenon essential for the correct description of narrow-gain-line lasers. In many such lasers, the selection of transverse modes is possible by tuning the length of the resonator. Then, the first and last terms on the right-hand side of Eq. (2) give the normal form of a supercritical Hopf bifurcation. When the control parameter $D_0 - 1$ goes through zero, a bifurcation occurs, characterized by a fixed amplitude but an arbitrary phase.

For class B lasers (e.g., ruby, Nd, and CO_2): $\gamma_\perp \gg \gamma_\prod \approx \kappa$, only the polarization intensity can be adiabatically eliminated. Then, its dynamic behavior is described by two coupled nonlinear equations corresponding to the light field and the population as follows:[76]

$$\begin{cases} \frac{\partial E}{\partial \tau} = (D - 1)E - i(\beta - d\nabla^2)E - g(\beta - d\nabla^2)^2 E \\ \frac{\partial D}{\partial \tau} = -\gamma_\prod[(D - D_0) + |E|^2 D] \end{cases}. \tag{3}$$

The first equation of Eq. (3) is the CSH dissipation equation suitable for class B lasers, where the higher-order diffusion term explains the choice of transverse modes. Comparing Eqs. (2) and (3), it can be found that in Eq. (3), the population D is the recovery variable and the fast light field E is the excitable variable. The overall particle inversion speed is slow, and the CSH equation contains additional nonlocal terms responsible for spatial mode selection, which will lead to the instability of pattern formation.

For class A and class B lasers, the output is stable in the absence of external disturbances. To realize an unstable operation, at least one degree of freedom needs to be added. The usual methods are as follows:[155–157] (1) modulate a certain parameter, such as the external field, pump rate, or cavity loss, to make the system a non-self-consistent equation system [Fig. 2(c)]; (2) inject the external field to increase the degrees of freedom of the system; (3) apply a two-way ring laser. In this case, the two backpropagating modes are coupled to each other, so that the number of degrees of freedom of the system is greater than two. Moreover, under the same conditions, observing the pattern formation of class B lasers will reveal two phenomena: periodic dynamics and low-dimensional deterministic chaos[76] [Fig. 2(e)]. Accordingly, fixed patterns and weak turbulence are the characteristics of class A laser output patterns[74] [Fig. 2(d)].

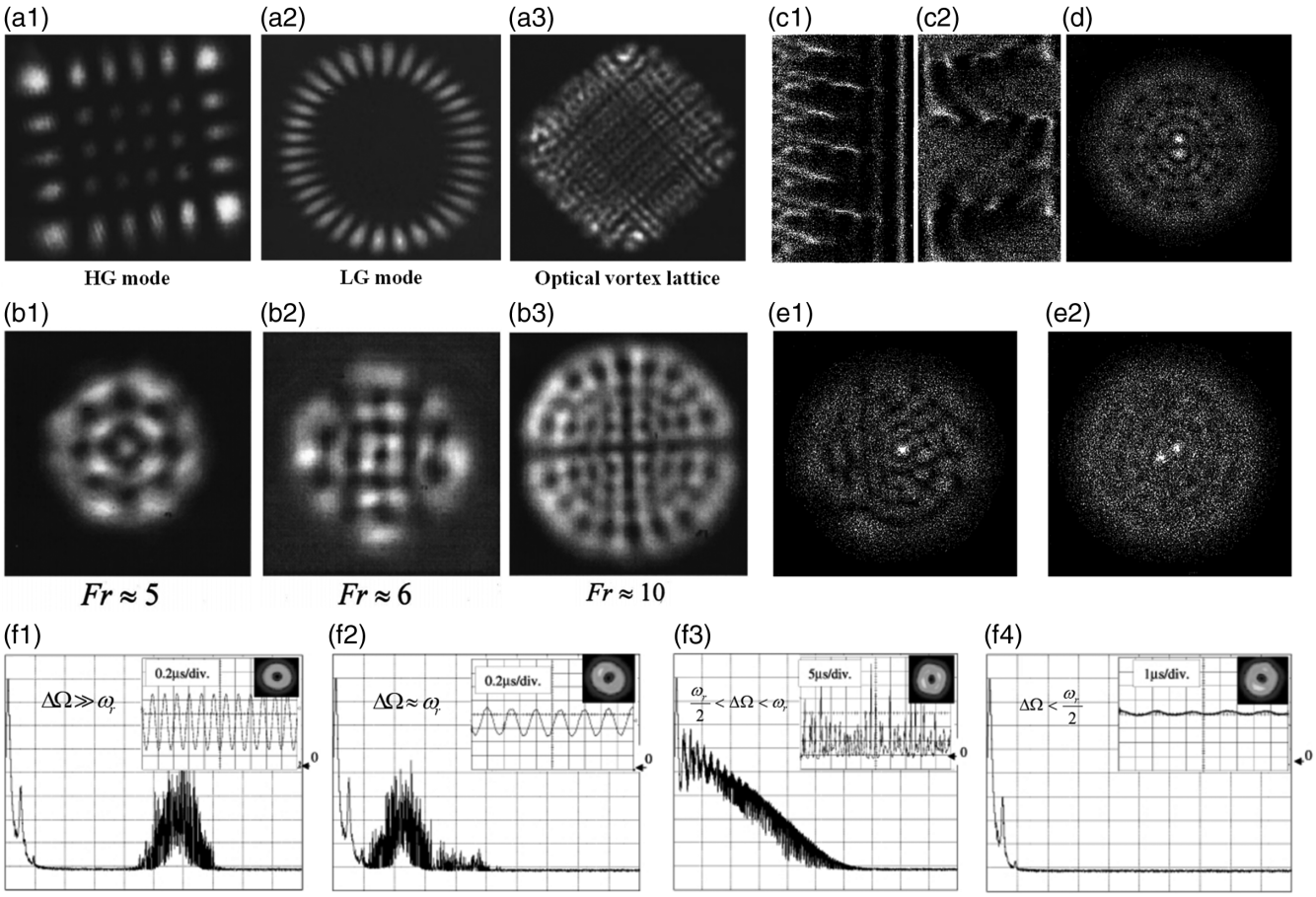

Fig. 2 Pattern formation and time-domain properties of classes A and B lasers in specific cases. (a) Laser transverse patterns are obtained by numerically solving the MB equations. Adapted from Ref. 84. (b) Laser OL patterns with different Fresnel numbers. Adapted from Ref. 85. (c) 1D nonstationary periodic (c1) and chaotic (c2) pattern in class A lasers when the pump gain is too high. Adapted from Ref. 74. (d) 2D stationary pattern in class A lasers. (e) 2D transient nonstationary pattern (e1) and time-averaged stationary pattern (e2) in class B lasers. (d)–(e) Adapted from Ref. 76. The corresponding principle between (e1) and (e2) was discussed in Ref. 77. (f) Different time-domain properties of laser pattern formation: self-modulated periodic oscillation (f1), self-modulated quasi-periodic oscillation (f2), chaotic pulsing (f3), and single-mode stable pattern (f4). Adapted from Ref. 153.

In addition, Huyet et al.[77] used multi-scale expansion to derive the CSH equation of the laser. They obtained two fields' equations: one is mainly caused by the phase fluctuations of the KS equation called the turbulent state,[158] while the other CSH equation produces periodic modulation in spatial and temporal intensities. The reason that the laser intensity is locally chaotic is explained by this system of equations, while the time-averaged intensity pattern maintains the overall symmetry of the system. The time-domain dynamics of laser pattern formation were further studied by Chen and Lan.[153,159] The ring beam distributed pumping technology is used to obtain the high-order $LG_{0,l}$ pattern. By slightly adjusting the spherical output coupling mirror, i.e., controlling the frequency difference $\Delta\Omega$ of the two $LG_{0,l}$ patterns, the relationship between $\Delta\Omega$ and the relaxation oscillation frequency ω_r of the solid-state laser is constantly changing, accounting for the different time-domain properties [Fig. 2(f)].

In summary, the derivation and deformation of the MB equations have laid the physical foundation for the spontaneous organization of spatial patterns of structured laser beams. The formation of one-dimensional (1D) and two-dimensional (2D) spatial patterns can be explained by solving the MB equations and its modified CGL, CSH, and KS equations under specific conditions. In addition, since the MB equations are a system of multivariate nonlinear equations in space and time, the time-domain properties of certain cases in laser pattern formation, such as stability, oscillation, and chaos, can also be described.

3 Eigenmode Superposition-Based Pattern Formation

Since structured laser beams often appear as time-averaged patterns in practical applications,[76,77,86] their spatial characteristics have received much attention in recent years. Here, we should refer to the Helmholtz equation,[90–96] which is the basic wave equation that the electric vector of optical frequency electromagnetic field should satisfy under the scalar field approximation. Generally, both the Helmholtz equation and MB equations can

describe the formation dynamics of laser spatial patterns, while the difference is that the former does not contain the temporal term, and the latter is a set of spatiotemporal equations. Hence, for the analysis of spatial characteristics of laser transverse patterns, it is more common to solve the Helmholtz equation,

$$\nabla^2 E + k^2 E = 0, \tag{4}$$

where ∇^2 is the Laplacian operator, E refers to the light field, and $k = 2\pi/\lambda$ is the light-wave number.

3.1 Eigenmodes of Helmholtz Equation

The Gaussian beam is a special solution of the Helmholtz equation under gradually varying amplitude approximation, which can describe the properties of laser beams well.[96] The Helmholtz equation can then be solved for several structured laser beams based on the Gaussian beam. First and foremost, by solving the Helmholtz equation in the paraxial form, i.e., the paraxial wave equation, the well-known HG and LG modes can be solved in Cartesian coordinates and cylindrical coordinates, respectively, as shown in Figs. 3(a)–3(b).[162,163] The IG modes are also an important family of orthogonal solutions to the paraxial wave equation, which represents a continuous transition from LG to HG modes, as shown in Fig. 3(c).[164–166] Another set of solutions to the Helmholtz equation in free space, when solved in cylindrical coordinates, is the Bessel modes, as shown in Fig. 3(e).[92,167,168] If solving the Helmholtz equation in elliptical cylindrical coordinates, Mathieu–Gauss beams can be obtained, as shown in Fig. 3(d).[169–171] Mathieu–Gauss beams are also one class of "nondiffracting" optical fields, which are a variant of the superposition of Bessel beams. Therefore, they have a similar capability of self-reconstruction after an opaque finite obstruction. Another important solution to the paraxial wave equation is the Airy beam, as shown in Fig. 3(f).[172,173] Similar to the Bessel modes, Airy beams exhibit unique properties of self-acceleration, nondiffraction, and self-reconstruction. Next, when solving the Helmholtz equation in parabolic coordinates, parabolic beams can be obtained, as shown in Fig. 3(g).[160] Their transverse structures are described by parabolic cylinder functions, and contrary to Bessel or Mathieu beams, their eigenvalue spectra are continuous. Any nondiffracting beam can be constructed as a superposition of parabolic beams, since they form a complete orthogonal set of solutions of the Helmholtz equation. Based on parabolic beams, a new family of vector beams that exhibit novel properties is explored, i.e., parabolic-accelerating vector beams, as shown in Fig. 3(h).[161] This set of beams obtains the ability to freely accelerate along parabolic trajectories. In addition, their transverse polarization distributions only contain polarization states oriented at exactly the same angle, but with different ellipticity. To sum up, the above-solved patterns we introduced are the eigenmodes of Helmholtz equations, with some examples shown in Fig. 3.

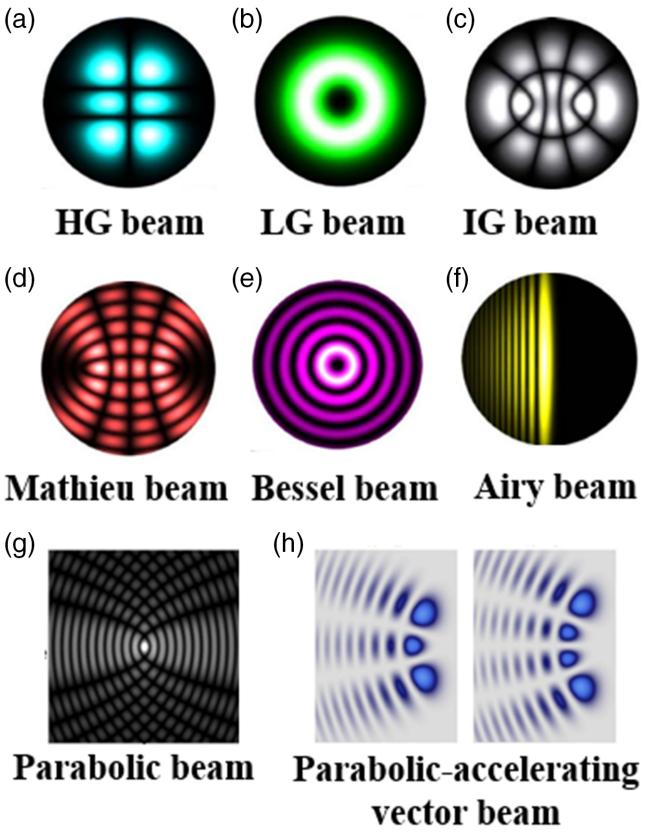

Fig. 3 Basic types of transverse patterns. (a) HG beam. (b) LG beam. (c) IG beam. (d) Mathieu beam. (e) Bessel beam. (f) Airy beam. (a)–(f) are adapted from Ref. 42. (g) Parabolic beam. Adapted from Ref. 160. (h) Parabolic-accelerating vector beam. Adapted from Ref. 161.

3.2 Eigenmodes Superposition Theory

For eigenmode superposition theory, it was found that the LG mode can be generated by coherent superposition of the HG modes as early as 1992,[90] as shown in Fig. 4(a). It can be conveniently understood by illustrating the above basic modes on a Bloch sphere, analogous to the Poincaré sphere (PS) for polarization, but for spatial modes. For example, if such a Bloch sphere is constructed with the LG_p modes, such as $\mathrm{LG}_{0,1}$ and $\mathrm{LG}_{0,-1}$ on the poles, then the equator will represent superpositions of such beams: the HG modes.[179] Due to the fact that these set of modes form an infinite basis, it allows one set of modes to be represented in terms of the other. Using relations between Hermite and Laguerre polynomials,[90,180]

$$\sum_{k=0}^{m+n} (2i)^k P_k^{(n-k,m-k)}(0) H_{n+m-k}(x) H_k(y) = 2^{m+n} \times \begin{cases} (-1)^m m!(x+iy)^{n-m} L_m^{n-m}(x^2+y^2) & \text{for } n \geq m \\ (-1)^n n!(x-iy)^{m-n} L_m^{m-n}(x^2+y^2) & \text{for } m > n \end{cases}, \tag{5}$$

$$P_k^{(n-k,m-k)}(0) = \frac{(-1)^k}{2^k k!} \frac{d^k}{dt^k} [(1-t)^n (1+t)^m]|_{t=0}, \tag{6}$$

where $H_k(\cdot)$ and $L_m^{n-m}(\cdot)$ are Hermite and Laguerre polynomials, respectively, then LG modes could be represented in terms of superpositions of HG modes as[181]

$$\mathrm{LG}_{p,\pm l}(x,y,z) = \sum_{K=0}^{m+n} (\pm i)^K b(n,m,K) \cdot \mathrm{HG}_{m+n-K,K}(x,y,z), \tag{7}$$

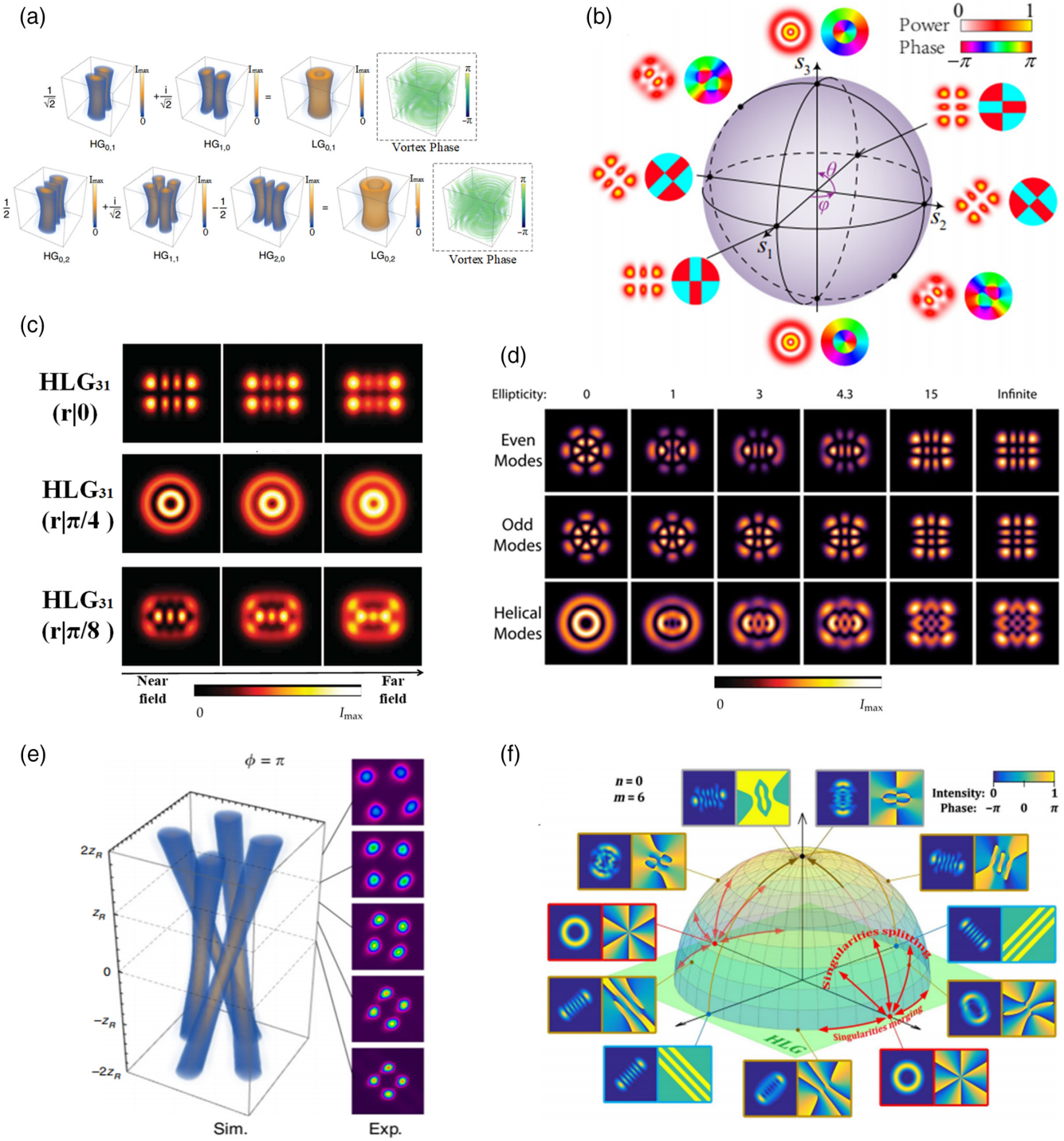

Fig. 4 Multiple types of transverse patterns after superposition. (a) Examples of the LG modes superposed of the HG modes. Adapted from Ref. 50. (b) HLG modes in PS. Adapted from Ref. 174. (c) The intensity distribution of HLG_{31} modes with different values of α. Adapted from Ref. 175. (d) The intensity distribution of even odd IG mode with $p = 5$ and $m = 3$, and the HIG mode generated by the corresponding superposition when $\varepsilon = 0 \to \infty$. Adapted from Ref. 176. (e) The vortex SU(2) geometric modes. Adapted from Ref. 177. (f) The intensity and phase distribution of SHEN modes for $(n, m) = (0,6)$. Adapted from Ref. 178.

$$b(n.m,K)=\left[\frac{(N-K)!K!}{2^N n!m!}\right]^{1/2}\frac{1}{K!}\frac{\mathrm{d}^K}{\mathrm{d}t^K}[(1-t)^n(1+t)^m]|_{t=0}, \tag{8}$$

where $l=m-n$, $p=\min(m,n)$, and $N=m+n$. This leads to an alternative description of light fields through the perspective of mode superposition, particularly useful in the description of beams with a transverse profile that is invariant during propagation. For the mutual superposition and conversion of HG and LG eigenmodes, Abramochkin and Volostnikov in 2004 introduced a parameter α to unify them.[182] Such beams with more universality are called generalized Gaussian beams or Hermite–Laguerre–Gaussian (HLG) beams.[41,175,182,183] The expression of HLG beam is as follows:

$$\mathrm{HLG}_{n,m}(\mathbf{r},\mathrm{z}|\alpha)=\frac{1}{\sqrt{2^{N-1}n!m!}}\exp\left(-\pi\frac{|\mathbf{r}|^2}{w}\right)\mathrm{HL}_{n,m}\left(\frac{\mathbf{r}}{\sqrt{\pi}w}|\alpha\right)\times\exp\left[ikz+ik\frac{\mathbf{r}^2}{2R}-i(m+n+1)\Psi(z)\right], \tag{9}$$

where $\mathrm{HL}_{n,m}(\bullet)$ are Hermite–Laguerre (HL) polynomials, $\mathbf{r}=(x,y)^{\mathrm{T}}=(r\cos\phi,r\sin\phi)^{\mathrm{T}}$, $R(z)=(z_R^2+z^2)/z$, $kw^2(z)=2(z_R^2+z^2)/z_R$, $\Psi(z)=\arctan(z/z_R)$, and z_R is the Rayleigh range. It was found that when $\alpha=0$ or $\pi/2$, the mode $\mathrm{HLG}_{n,m}$ will be reduced to $\mathrm{HG}_{n,m}$ or $\mathrm{HG}_{m,n}$ mode. When $\alpha=\pi/4$ or $3\pi/4$, the mode $\mathrm{HLG}_{n,m}$ will be reduced to $\mathrm{LG}_{p,\mp l}$ mode $[p-\min(m,n),l=m-n)]$. For other α, the mode $\mathrm{HLG}_{n,m}$ is displayed as the beam distribution of multi-phase singularities. Take $\mathrm{HLG}_{3,1}$ mode as an example, when $\alpha=0$, $\pi/4$, and $\pi/8$, the mode $\mathrm{HLG}_{3,1}$ could be reduced to HG_{31}, LG_{12}, and mode with multi-phase singularities, as shown in Fig. 4(c).[175] Since HLG modes are able to unify HG modes and LG modes, it was mapped in the PS to show the relationship among HLG, HG, and LG modes.[174] As shown in Fig. 4(b), the poles represent the high-order LG modes with opposite topological charges, and the equator represents the high-order HG modes, while the mode between the poles and the equator represents the transitional high-order HLG modes.

On the basis of HLG modes, analyzing its coherent superposition can obtain a high-dimensional complex light field in a coherent state, whose typical type is SU(2) mode. The SU(2) mode appears when the laser mode undergoes frequency degeneracy with a photon performing as an SU(2) quantum coherent state coupled with a classical periodic trajectory,[174,177,184,185] which contains both spatially coherent wave packets and geometric ray trajectories, as shown in Fig. 4(e). Taking the HLG mode as the basic mode of SU(2) coherent state, the superposed SU(2) mode is expressed as[174]

$$|\psi_{n,m,l}^{N,P,Q}\rangle=\frac{1}{2^{N/2}}\sum_{K=0}^{N}e^{iK\phi}\binom{N}{K}^{\frac{1}{2}}|\psi_{n+QK,m,l-PK}\rangle, \tag{10}$$

where ϕ is the phase term, and P/Q (P and Q are coprime integers) is the ratio of the distance between the transverse mode and longitudinal mode leading to frequency degeneracy, i.e., the transverse mode and longitudinal mode of various eigenmodes should meet the coherent superposition condition.

Another similar superposition of the IG modes can form patterns with multi-singularity, named the helical IG (HIG) modes.[186–188] HIG modes are obtained by coherent superposition of even and odd IG modes, whose expression is

$$\mathrm{HIG}_{p,m}^{\pm}=\mathrm{IG}_{p,m}^{e}(\xi,\eta,\varepsilon)\pm i\mathrm{IG}_{p,m}^{o}(\xi,\eta,\varepsilon), \tag{11}$$

where $\pm$ is the direction of the vortex; p and m are the orders of the IG mode; o and e represent the odd mode and the even mode, respectively; ε is the ellipticity parameter, indicating the change degree of ellipticity. ξ and η are elliptic coordinates; and $\mathrm{IG}_{p,m}^{e,o}(\cdot)$ represent the expression of IG modes.[165] When $\varepsilon\to 0$, $\mathrm{IG}_{p,m}^{e,o}$ modes could be reduced to $\mathrm{LG}_{p,l}$ modes with $l=m$ and $p=2n+l$. When $\varepsilon\to\infty$, $\mathrm{IG}_{p,m}^{e,o}$ modes could be reduced to HG_{n_x,n_y} modes with $n_x=m-1$ and $n_y=p-m+1$. Therefore, for $\varepsilon=0\to\infty$, the HIG modes composed of even and odd modes show specific distribution changes, shown in Fig. 4(d).[176]

Comparing HLG and HIG modes, it could be found that they all possess phase singularities with corresponding spatial distributions for differently composed HG and LG modes. The above HG, LG, HLG, and HIG modes belong to the general family of structured Gaussian modes, also known as the singularities hybrid evolution nature (SHEN) modes.[178] The model expression of SHEN modes is

$$\mathrm{SHEN}_{n,m}(x,y,z|\beta,\gamma)=\sum_{K=0}^{N}e^{i\beta K}b(n,m,K)\bullet\begin{cases}(-i)^K\mathrm{IG}_{N,N-K}^{e}(x,y,z|\varepsilon=2/\tan^2\gamma, & \text{for } (-1)^K=1\\ (-i)^K\mathrm{IG}_{N,N-K+1}^{o}(x,y,z|\varepsilon=2/\tan^2\gamma, & \text{for } (-1)^K\neq 1\end{cases}. \tag{12}$$

When $\beta=\pm\pi/2$, SHEN modes could be reduced to HIG modes. When $\gamma=0$, SHEN modes could be reduced to HLG modes. When $(\beta,\gamma)=(0,0)$ or $(\pi,0)$, SHEN modes could be reduced to HG modes. When $(\beta,\gamma)=(\pm\pi/2,0)$, SHEN modes could be reduced to LG modes. Therefore, SHEN modes can uniformly describe HG, LG, HIG, and HLG modes. In addition, the PS could be applied to define the SHEN sphere to describe these modes, as shown in Fig. 4(f).[178]

It can be seen that the above patterns are derived from the direct coherent superposition of the basic modes. The beam generated after superposition can be regarded as a new kind of eigenmodes with single-frequency operation. If performing coherent superposition between these eigenmodes, diverse and complex structured laser beam patterns could be generated. Moreover, in a practical resonator, if multiple modes interact coherently, the coupling of frequency and phase will be formed spontaneously to achieve TML. The principle of the TML effect[97–101] includes frequency locking and phase locking. The total electric field of a beam in the coherent superposition state can be given as[99]

$$E_{\mathrm{tot}}=\sum_{m,n}a_{m,n}XG_{m,n}(\cdot)*\exp\left[i\phi_{m,n}+ikz+ik\frac{x^2+y^2}{R(z)}-iq\psi(z)\right], \tag{13}$$

where XG represents the polynomial of eigenmodes, such as HG, LG, and IG. The subscripts m and n are the order indices of the corresponding basic modes, $a_{m,n}$ is the weight of each basic mode, $\exp(\ldots)$ is the phase item, $\phi_{m,n}$ is the initial phase, and $q\psi(z)$ is the Gouy phase.

The spatial pattern is analyzed by superimposing the electric field of multiple modes with the locking phase, including the Gouy phase.[189] Moreover, with the assistance of the inherent nonlinearity of the laser cavity, the frequencies of the composed modes are possible to be pulled to the same value,[87–89] and then the total electric field can be expressed as

$$E_{\mathrm{tot}}(x,y,z) = \exp\left[i\frac{\overline{\omega}}{c}z + i\frac{\overline{\omega}}{c}\frac{x^2+y^2}{\overline{R(z)}} - i\overline{q}\psi(z)\right] \cdot \sum_{m,n} a_{m,n} XG_{m,n}(\cdot) * \exp(i\phi_{m,n}), \tag{14}$$

where $\overline{\omega}$ is the averaged optical frequency, whose derivation is as follows:

$$\begin{cases} \overline{\omega} = \omega_0 + \dfrac{\sum_{m,n} a_{m,n}\Delta\omega_n}{\sum_{m,n} a_{m,n}} \\ \Delta\omega_n = \omega_n - \omega_0 = \dfrac{c(k_x^2+k_y^2)}{2k_z} \end{cases}. \tag{15}$$

Here, ω_0 is the optical frequency of the fundamental transverse mode, $\Delta\omega_n$ is the frequency spacing between the nth mode and the fundamental mode, c is the velocity of light, $k_x = \pi n/l_x$, $k_y = \pi n/l_x$, $k_z = 2\pi/\lambda$, and l_x and l_y are the sizes of the cavity in the x and y directions, respectively. Along with the locking of frequencies, the parameters of $R(z)$ and index of $\psi(z)$ should also be an averaged one to help with the locking of the total phases. The cooperatively frequency-locked multimode regime, in which at least two transverse modes contribute significantly to the output field, and lock to a common frequency with which they oscillate in a synchronized way. The locking concerns also the relative phases of the modes, so that the output intensity has a stationary transverse configuration. The common oscillation frequency, cooperatively selected by the modes, corresponds to the average of the modal frequencies, weighted over the intensity distribution of the modes in the stationary state.

The patterns formed by TML effect could possess phase singularities in dark points.[102] Around each of these phase singularities, the modulus of the electric field raises from zero in the form of an inverted cone with a steep gradient. If performing a closed counterclockwise loop that surrounds one of these points, the phase of the envelope of the electric field changes by a value equal to $\pm 2\pi m$, where m is a positive integer. These properties are fulfilled also in the "optical vortices" discovered by Coullet and collaborators[63] in their 2D analysis of the model.[62] A major difference is that from the fact that the vortices in Ref. 63 can be generated in any position of the transverse plane, whereas the singularities that appear in the stationary configurations of a laser system are located in precisely defined positions, i.e., the dark points.

The stable beam pattern formed by coherent superposition through TML usually needs to meet the following conditions: First, there should be a large value of the Fresnel number to sustain such multi-transverse modes.[85] Second, the transverse mode spacing, Δv_T, should be small (several gigahertz or lower) to assist nonlinear coupling in the spectral band.[190] Third, the interval between two neighboring vortices should also be small (usually tens of micrometers) for the formation of stable patterns.[191] Fourth, a wide cavity without mechanical boundaries is also needed.[87] The patterns produced by the eigenmode coherent superposition in the TML state include optical lattice (OL) and OVL,[86,88,89] which could be obtained in vertical-cavity surface-emitting lasers (VCSELs)[87] and solid-state lasers,[88,89,99,192] as shown in Figs. 5(a)–5(e). In addition to coherent superposition, incoherent superposition can also produce patterns similar to OL,[193,195] as shown in Figs. 4(f) and 4(g). The incoherent superposition is to analyze the output OL pattern through the superposition of intensities of the composed modes alone. It is pointed out that in multi-transverse-mode lasers, the coupling between transverse modes occurs through their intensities rather than their field amplitudes, and these modes are arranged according to the principle of transverse hole burning to maximize energy coexistence and minimize intensity distribution overlap. It is found that the beam patterns generated by incoherent superposition have higher symmetry, and there may be no phase singularity in some dark areas of the pattern.[194]

We have summarized the principle of directly generating spatially structured beams from the laser cavity, namely, the eigenmode superposition theory. The spatial characteristics of the spontaneous organized patterns are explained by the interaction and superposition of the oscillation modes. However, with the help of some modulation devices, such as the spiral phase plate,[196–198] diaphragm,[199] acousto-optic modulator,[200] liquid crystal Q-plate,[201–205] J-plate,[145] liquid crystal SLM,[206–208] and digital micromirror device,[209–211] various spatial structure laser beams can also be generated indirectly. There are also many reviews[40,42,43,45–47,50,212] on this part of active regulation to generate spatially structured laser beams, and more detailed information can be found in those reviews.

4 Spatiotemporal Beam Patterns

As for the study of structured laser pattern formation, the traditional electromagnetic field equations including MB and Helmholtz equations were adopted in recognition of the importance of gain and loss. In addition, the eigenmode superposition theory makes it possible to form diverse and complex beam patterns. When the laser oscillates simultaneously in multiple modes and the phase difference between them is stable, the mode locking occurs. What we talked about the spatial characteristics of laser transverse modes in Sec. 3 is to study the TML under the condition of single longitudinal mode. However, if multiple longitudinal modes are involved, total mode locking or spatiotemporal locking will occur,[103–106] thus generating spatiotemporal laser beams.

4.1 Spatiotemporal Mode Locking

The spatiotemporal mode locking is often realized by fiber lasers, referring to the coherent superposition of longitudinal and transverse modes of the laser, which allows locking multiple transverse and longitudinal modes to create ultrashort pulses with various spatiotemporal distributions, as shown in Figs. 6(a1) and 6(a2). The locking of transverse and longitudinal modes of a laser is realized by spatial filtering[107] and spatiotemporal normal dispersion mode locking,[116,117] respectively. The spatiotemporal mode locking can be realized through the high nonlinearity, gain, and spatiotemporal dispersion of the optical fiber medium, as well as spectral and spatial filtering.[103] These

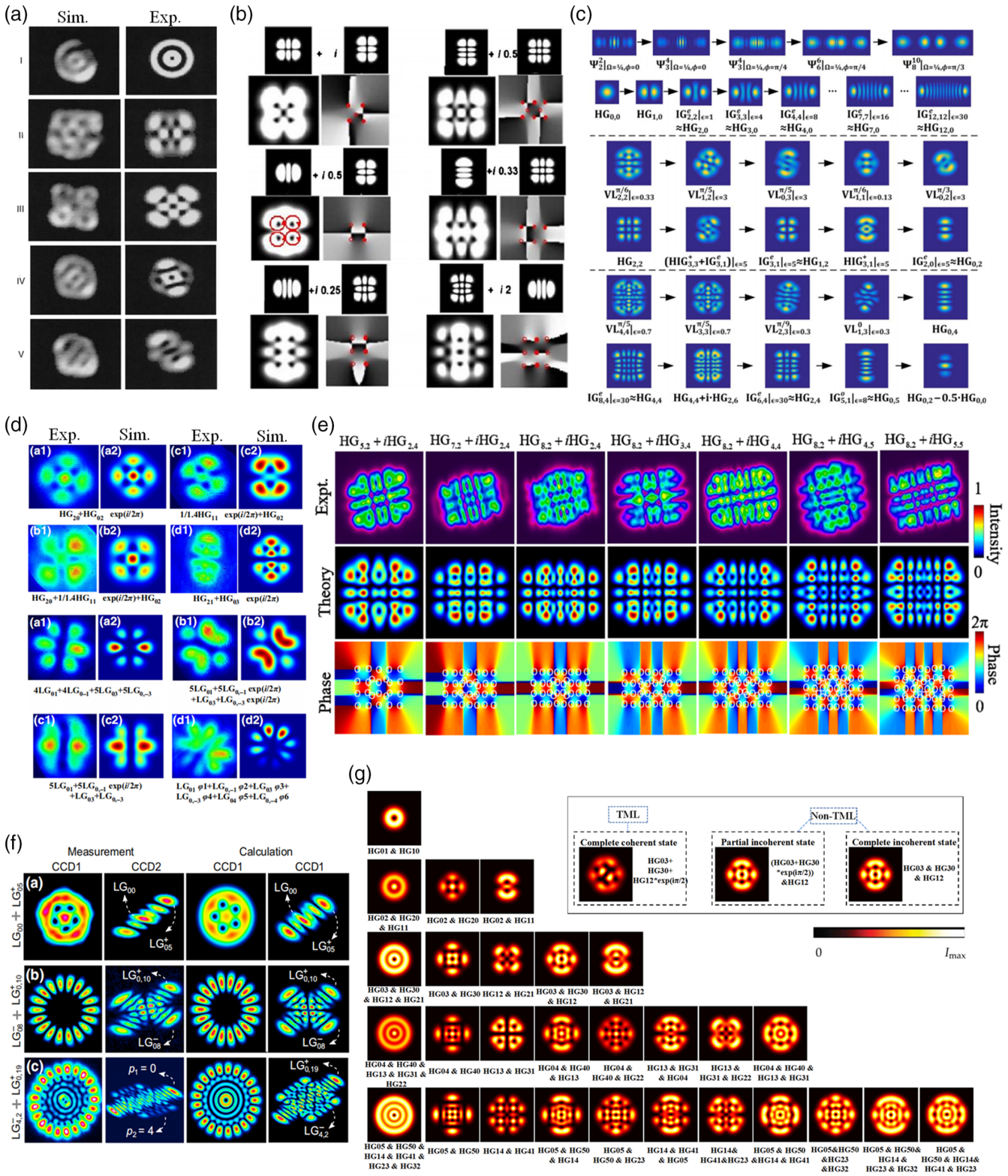

Fig. 5 Multiple patterns produced by coherent and incoherent superposition. (a)–(e) OVL patterns from coherent superposition of HG, LG, and IG modes, while (a) is from VCSELs. Adapted from Ref. 87. (b) Beam patterns from a solid-state LNP laser. Adapted from Ref. 88. (c) Beam patterns from a solid-state Yb:CALGO laser. Adapted from Ref. 89. (d) Beam patterns from a microchip Nd:YAG laser. Adapted from Ref. 99. (e) Beam patterns from a solid-state Pr:YLF laser. Adapted from Ref. 192. (f)–(g) Beam patterns from incoherent superposition of the (f) LG and (g) HG modes in solid-state lasers. Adapted from Refs. 193 and 194.

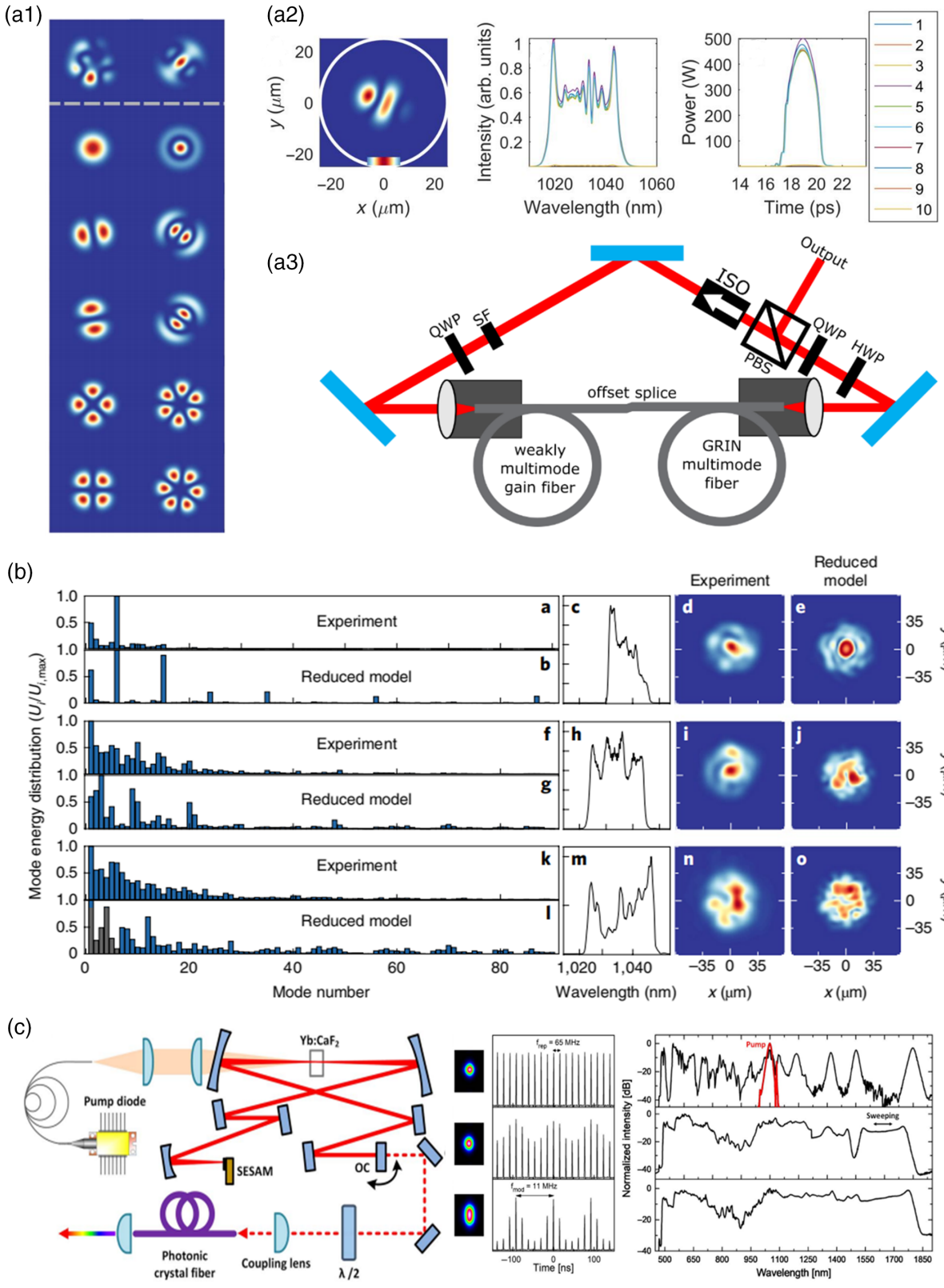

Fig. 6 Spatiotemporal mode-locking beam patterns. (a) Spatiotemporal mode locking through both longitudinal and transverse modes. Adapted from Ref. 103. (a1) Transverse distributions. (a2) Pattern, spectra, and intensity of composed modes. (a3) Schematic diagram of the cavity supporting spatiotemporal mode locking. (b) Experimental regimes of spatiotemporal mode locking and results from a reduced laser model. Adapted from Ref. 107. (c) Phase locking of the longitudinal and transverse (TEM_{00} and TEM_{01}) modes to create scanning beam. Adapted from Ref. 114.

inseparable coupling effects can be described by the cavity operator $\hat{C}$ as follows:[107]

$$\hat{C} = \hat{F}(x,y)\hat{F}(\omega)\widehat{SA}(x,y,t)\hat{P}(x,y,t), \tag{16}$$

where $\hat{F}(x,y)$ and $\hat{F}(\omega)$ are the spectral and spatial filter functions, respectively, $\widehat{SA}(x,y,t)$ is the spatiotemporal saturable absorber transfer function, and $\hat{P}(x,y,t)$ accounts for the effect of the pulse propagation through the three-dimensional (3D) nonlinear gain medium. $\hat{P}$ includes the inseparable effects of 3D gain, such as spatiotemporal dispersion and nonlinear mode coupling. With the composition of iterated nonlinear projection operations, the field of spatiotemporal locking pulse can be expressed as

$$E_{i+1}(x,y,t) = \hat{C}E_i(x,y,t), \tag{17}$$

where the subscript of E is the round-trip number. In each round trip, the nonlinear dissipation of $\hat{C}$ is selected from the field certain attributes, and the saturable laser gain provides a conditional (frequency and energy-limited, and spatially localized) rescaling of the selected field.

The schematic diagram of the cavity supporting spatiotemporal mode locking is shown in Fig. 6(a3). The fiber ring laser was composed by offset splicing a graded-index fiber to a few-mode (three modes were supported) Yb-doped fiber amplifier, which leads to spatial filtering action.[107] Spatial filtering can lock multiple transverse modes by controlling the overlap of fields coupled to the optical fiber. Then, the self-starting mode locking in the normal chromatic dispersion regime is achieved using a combination of spectral filtering and intracavity nonlinear polarization rotation, which is realized in the longitudinal mode locking. Through the space–time locking of the transverse and longitudinal modes, ultrashort pulses with special space–time distribution can be obtained. In the process of spatiotemporal mode locking, the mode dispersion will affect the locking effect, and the small mode dispersion of graded-index multimode fiber is considered to be a key factor to make spatiotemporal mode locking possible.[103] Experimental regimes of spatiotemporal mode locking and results from a reduced laser model are shown in Fig. 6(b).[107] The reduced models predicted how the effects of disorder, and the increased dimension of the optimization, affect the regimes of spatiotemporal mode locking. On this basis, it was found that spatiotemporal mode locking can also be realized in multimode fiber lasers with large mode dispersion, in which the intracavity saturable absorber plays an important role in offsetting the large mode dispersion.[110] Spatiotemporal mode locking at a fiber laser using a step-index few-mode thulium fiber amplifier and a semiconductor saturable absorber was also reported.[113] The former realizes spatial filtering to lock the transverse mode, and the latter plays a role in longitudinal mode locking.

Therefore, spatiotemporal mode locking is affected by gain, spatial filtering, optical nonlinear interaction between saturable absorbers, and optical fiber medium, as well as the coupling between temporal and spatial degrees of freedom.[107] Apart from multimode fiber lasers, in all few-mode fiber, it is realizable to obtain spatiotemporal mode locking to create bound-state solitons.[109] In addition, the scanning output beam can be generated by spatiotemporal locking of the laser mode,[114] as shown in Fig. 6(c). The phase locking of the longitudinal and transverse (TEM_{00} and TEM_{01}) modes is simply obtained by tilting the pump laser end mirror to induce time-varying pulse coupling in a photonic crystal fiber for subsequent generation of frequency-shifted Raman solitons. The introduced spatial oscillations of the output beam lead to modulation of the coupling efficiency of the fiber and effectively induces wavelength sweeping.

4.2 Spatial Modulation of Mode-Locked Laser Pulses

The spatiotemporal mode-locked pulses directly produced by fiber lasers are often irregularly distributed. Another method to generate spatiotemporal beams with regular and complex distribution is to use the pulse-shaping device based on SLM. The designed pulse shaper is usually applied to shape the input femtosecond laser to obtain the specific spatiotemporal pattern. As shown in Fig. 7(a), the spatiotemporal optical vortices have been proved to be generated using spiral phase in the pulse shaper.[118] Suppose an optical field in the spatial frequency–frequency domain $(k_x - \omega)$ is given by $g_R(r)$. After a spiral phase of $e^{-il\theta}$ is applied, a 2D Fourier transform gives the field in the spatial-temporal (x,t) domain as follows:

$$G(\rho,\phi) = \mathrm{FT}\{g_R(r)\mathrm{e}^{-il\theta}\} = 2\pi(-i)^l\mathrm{e}^{-il\theta}H_l\{g_R(r)\}, \tag{18}$$

where (r,θ) are the polar coordinates with $r = \sqrt{k_x^2+\omega^2}$ and $\theta = \tan^{-1}(\omega/k_x)$, and (ρ,ϕ) are the Fourier conjugate polar coordinates with $\rho = \sqrt{x^2+t^2}$ and $\theta = \tan^{-1}(x/t)$. Here, $H_1\{g_R(r)\} = \int_0^\infty r g_R(r)J_1(2\pi\rho r)\mathrm{d}r$ and J_l is the Bessel function of the first kind.

Therefore, starting from chirped mode-locked pulses, a diffraction grating and cylindrical lens disperse frequencies spatially and act as a time-frequency Fourier transform. Then, a spiral phase on the SLM and an inverse Fourier transform by recollecting dispersed frequencies with a grating-cylindrical lens pair form the chirped spatiotemporal vortex. The full electric field is presented as

$$E(\rho,\phi) = G(\rho,\phi)\exp(ik_z z - i\omega t). \tag{19}$$

After generating the spatiotemporal vortex pulse, it travels through an afocal cylindrical beam expander and stretches in the direction of the vortex line. It is reported that the stretched spatiotemporal vortex pulse could transform into a toroidal vortex pulse through a conformal mapping system formed by two SLMs,[126] as shown in Fig. 7(b). In addition, the spatiotemporal optical vortex was also demonstrated to be generated from a light source with partial temporal coherence and fluctuating temporal structures.[119] Similarly, through a phase mask in SLM, interesting wave packets, such as diffraction-free pulsed beams with arbitrary 1D transverse profiles without suffering power loss were generated.[121] The basic concept [illustrated in Fig. 7(c)] combines spatial-beam modulation and ultrafast pulse shaping and is related to the so-called $4f$-imager used to introduce spatiotemporal coupling into ultrafast pulsed beams. The modulated beam is reflected back, and the pulse is reconstituted by the grating to produce the spatiotemporal light sheet. Additionally, it applied reflective annular mask in a pulse shaper to generate a spatiotemporal Bessel wave packet,[122] as shown in Fig. 7(d). Since the mask has an annular shape, it is then possible to obtain a spatiotemporal Bessel beam at its waist by doing the inverse Fourier transform in the space and time domains of the signal

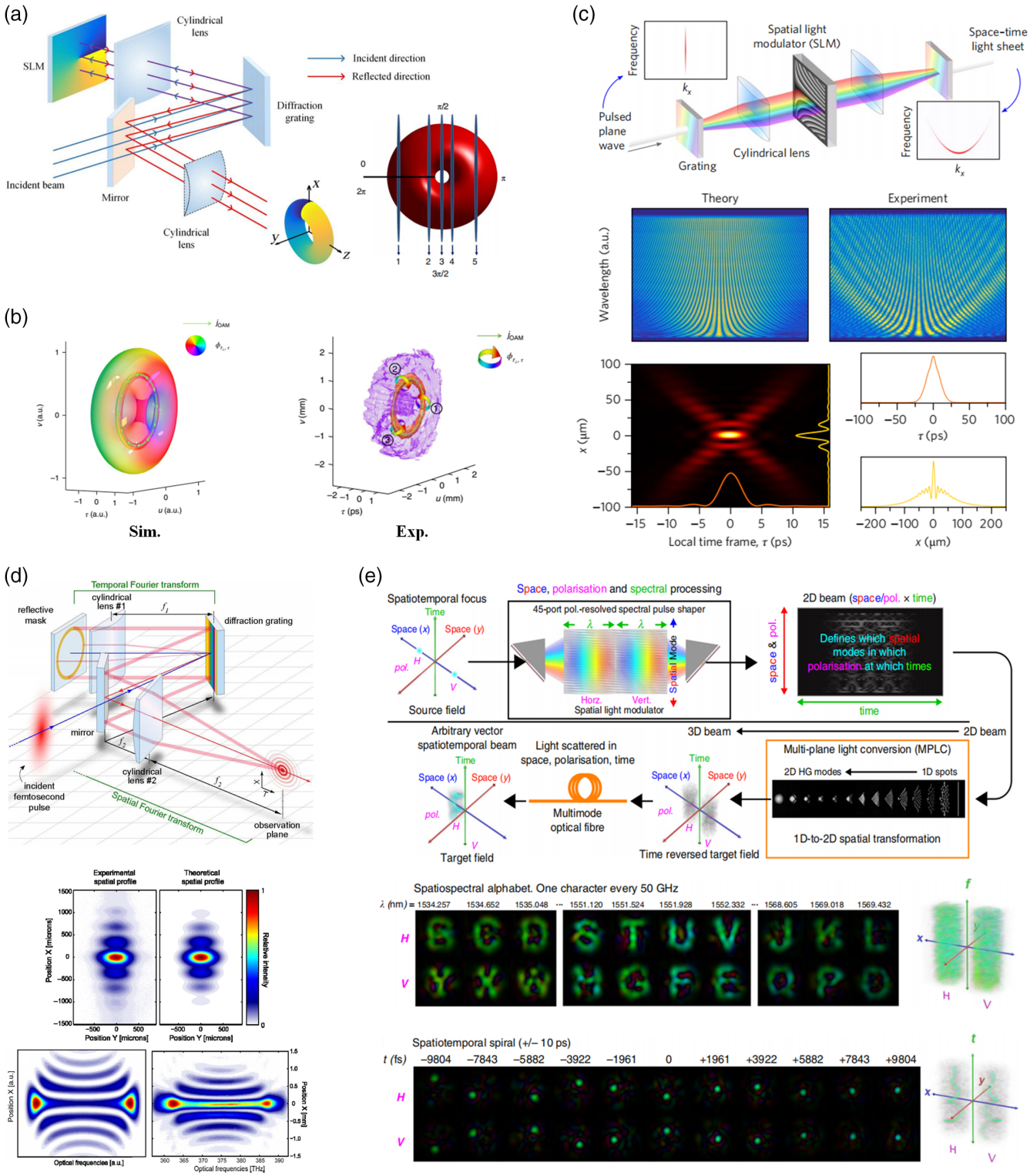

Fig. 7 Spatiotemporal beam patterns generated by a pulse shaper. (a) Generation (a1) and measurement (a2) of the spatiotemporal vortex. Adapted from Ref. 118. (b) Generation of the spatiotemporal toroidal vortex. Adapted from Ref. 126. (c) Generation of spatiotemporal Airy beams. Adapted from Ref. 121. (d) Generation of spatiotemporal Bessel beams. Adapted from Ref. 122. (e) Schematic of a device capable of mapping an input vector spatiotemporal field onto an arbitrary vector spatiotemporal output field. Adapted from Ref. 125.

reflected by the mask. This analysis has revealed that these beams are produced by a superposition of plane waves of different optical frequencies and directions of propagation traveling at the same group velocity along the z axis. With all plane waves added in the same phase, a nondiffraction spatiotemporal beam can be generated through spatiotemporal coupling.[124]

In addition, a device for generating an arbitrary vector spatiotemporal light field with arbitrary amplitude, phase, and polarization at each point in space and time was designed.[125] As shown in Fig. 7(e), the laser output with two orthogonal polarizations propagates through the pulse shaper to redistribute between the space domain and the time domain. The shaped light propagates through the multi-plane light conversion (MPLC) device and is converted to different HG modes at the output port of the MPLC. Then, arbitrary spatiotemporal beams can be generated through the design and combination of HG beams at different times. These methods of transforming spatiotemporal beams through optical devices, such as pulse shapers, gratings, and lenses can effectively generate spatiotemporal beams with specific structures. They can be used in the fields of imaging, optical communication, nonlinear optics, particle manipulation, and so on.

5 Structured Beam Patterns Generated by Nonlinear Processes

For the booming research on the spatial and spatiotemporal properties of structured laser beams reviewed in the above sections, investigations are based on beams at a single wavelength. Currently, the nonlinear transformation technology for fundamental mode Gaussian beams is very mature. The combination between structured laser beams and nonlinear transformation on the transverse pattern variation has been of great interest in recent years. The SFG,[127–130] SHG,[131–140] FWM,[141,142] and other frequency upconversion[143–145] methods have been studied in the nonlinear process of structured laser beams. The variation of OAM in the nonlinear process are one of the focuses of these studies. In this section, the nonlinear process of structured laser beams is introduced from two aspects: external-cavity modulations and intracavity transformation. We will first present the physical mechanisms.

Generally, the nonlinear transformation of structured patterns is based on the nonlinear wave equation,

$$\frac{\partial E}{\partial z} = \frac{i\omega}{2\varepsilon_0 cn} P^{\mathrm{NL}} e^{i\Delta k z}, \tag{20}$$

where E is the electric field, ω is the optical frequency, P^{NL} is the nonlinear polarization, and Δk is the wave vector difference between the polarized wave and the incident light. The nonlinear process in the multi-wave mixing process can be obtained by solving the coupled wave equations. Generally speaking, for the n'th-order nonlinear effect, $n+1$ nonlinear coupled wave equations corresponding to different frequencies can be listed. By simultaneously solving the $n+1$ coupled wave equations, the electric field strengths of these different frequencies of light can be obtained, thereby leading to the law of mutual conversion of energy between these light fields. In the nonlinear transformation of structured patterns, the second-order nonlinear effect is the main part, including SFG and SHG. Consider three monochromatic plane waves E_1, E_2, and E_3 propagating in the z direction with frequencies ω_1, ω_2, and ω_3, respectively. Considering only the second-order nonlinear effect, the second-order nonlinear polarization can be written as

$$\begin{cases} P^{(2)}(\omega_1) = 2\varepsilon_0 \chi^{(2)}(-\omega_1;\omega_3,-\omega_2)\cdot E_3 E_2^* \\ P^{(2)}(\omega_2) = 2\varepsilon_0 \chi^{(2)}(-\omega_2;\omega_3,-\omega_1)\cdot E_3 E_1^* \\ P^{(2)}(\omega_3) = 2\varepsilon_0 \chi^{(2)}(-\omega_3;\omega_1,\omega_2)\cdot E_1 E_2 \end{cases}, \tag{21}$$

and we can get the coupled wave equations for three-wave interaction as

$$\begin{cases} \frac{dE_1(z)}{dz} = \frac{i\omega_1}{cn_1}\chi^{(2)}(-\omega_1;\omega_3,-\omega_2)\cdot E_3(z)E_2^*(z)e^{i\Delta k z} \\ \frac{dE_2(z)}{dz} = \frac{i\omega_2}{cn_2}\chi^{(2)}(-\omega_2;\omega_3,-\omega_1)\cdot E_3(z)E_1^*(z)e^{i\Delta k z} \\ \frac{dE_3(z)}{dz} = \frac{i\omega_3}{cn_3}\chi^{(2)}(-\omega_3;\omega_1,\omega_2)\cdot E_1(z)E_2(z)e^{i\Delta k z} \end{cases}. \tag{22}$$

Then, the field intensity of a specifically structured light beam after nonlinear transformation can be obtained by substituting the structured light field expression XG (e.g., HG, LG, and IG) into the coupled wave Eq. (22) and solving them.

5.1 External Cavity Nonlinear Processes

External cavity pattern modulations and nonlinear interactions are the main form of nonlinear transformation in structured laser beams. The first research on the transformation of structured laser beams in nonlinear optics began with the SHG of LG modes in 1996.[131] It was found that the SHG fields carry twice the azimuthal indices of the pump, which provided straightforward insight into OAM conservation during nonlinear interactions at the photon level. The relationship among the OAMs of the input $l_1, l_2, \ldots$ and output beams l was recognized to follow the law of $l = l_1 + l_2 + \ldots + l_n$. That is, OAM is conserved in the nonlinear process. As such, for SHG modes of two photons with angular frequency ω and a single OAM, if the OAMs are equal, it has $l_{2\omega} = 2l_\omega$ or $l_{2\omega} = l_{\omega'} + l_{\omega''}$,[135] as shown in Fig. 8(a). This conservation law is also applicable to fractional and odd-order OAM beams.[134] The generation of LG beams with higher radial orders and IG beams through a nonlinear wave mixing process was further investigated to obtain more complex beam patterns.[130,139,140] However, in the above studies, the characteristics of the frequency-doubled beam patterns during propagation have hardly been mentioned. Later, in the research of SHG modes through input LG beams with opposite OAMs, the near- and far-field patterns show different light field distributions,[137] as shown in Fig. 8(b). In addition, for the change of pattern transmission, a more detailed theoretical model is proposed to describe the beam pattern transmission and radial mode transition in the process of SHG, and the results agree well with the simulations,[145] as shown in Fig. 8(c). Apart from the single OAM state, phase structure transfer in FWM[142] and sum frequency129 processes were also investigated for the input beams possessing coherent superposition of LG beams.

As shown in Fig. 8(d), there are two sets of patterns and propagation behaviors: (1) one pump beam carries OAM superposition mode with another pump beam carrying a single OAM mode and (2) both pump beams carry OAM superposition modes. The relationship between the SFG beam and the pump beam is as follows:[129]

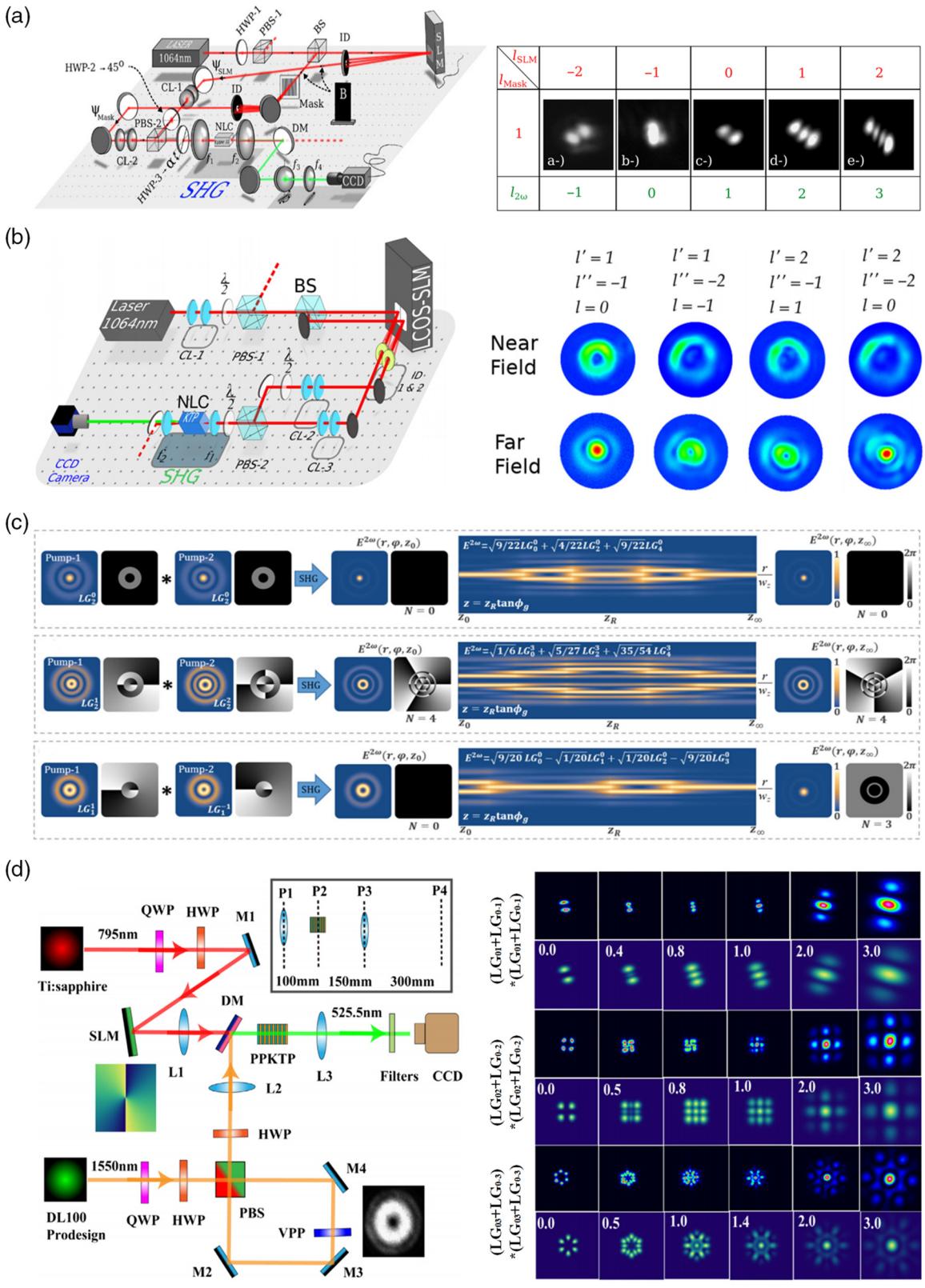

Fig. 8 External cavity nonlinear process of structured laser beams. (a) Experimental setup and results showing the OAMs of the input and output beams are equal. Adapted from Ref. 135. (b) Experimental setup and results showing different SHG pattern distributions in near and far fields. Adapted from Ref. 137. (c) SHG patterns with beam pattern transmission and radial mode transition. Adapted from Ref. 145. (d) Experimental setup and results of SFG modes with input beams possessing coherent superposition of LG beams. Adapted from Ref. 129.

$$E_{\mathrm{SFG}} \propto \begin{cases} (LG_0^l + e^{i\theta} LG_0^{-l}) * LG_0^l \rightarrow LG_0^{2l} + e^{i\theta} LG_l^0 \\ (LG_0^{l_1} + e^{i\theta} LG_0^{-l_2}) * LG_0^{l_2} \rightarrow LG_0^{l_1+l_2} + e^{i\theta} LG_{l_2}^0 \\ (LG_0^l + e^{i\theta_1} LG_0^{-l}) * (LG_0^l + e^{i\theta_2} LG_0^{-l}) \rightarrow LG_0^{2l} \\ + e^{i(\theta_1+\theta_2)} LG_0^{-2l} + (e^{i\theta_1} + e^{i\theta_2}) LG_l^{*0} \end{cases}, \tag{23}$$

where LG_0^l represents the standard LG mode, and θ is the phase item. It is worth noting that LG_l^{*0} is similar to the standard LG mode LG_l^0, but differs by a factor of 2 in the Laguerre polynomials. This difference makes the intensity in the radial direction of the SFG beam decrease much more rapidly than the standard LG mode.

5.2 IntraCavity Nonlinear Processes

All these above studies on nonlinear processes were explored on the basis of external cavity structured laser pattern generation. Usually, in these studies, structured beams were first generated with the help of modulation devices (such as SLM), and then frequency conversion was carried out. For patterns generated through intracavity nonlinear process, some studies showed new properties. In Fig. 9(a1), it shows a frequency-doubled cavity that converts the infrared fundamental frequency of Nd:YAG ($\lambda = 1064$ nm) to the second-harmonic green ($\lambda = 532$ nm) through an intracavity nonlinear crystal (KTP).[146] The concept of the laser design exploits a unique feature of OAM coupling to linear polarization states. The resonant mode morphs from a linearly polarized Gaussian-like enveloped beam at one end of the cavity to an arbitrary angular momentum state at the other. A polarizer was required for selection of the horizontal polarization state before the J-plate, and the polarization of the light traversing the J-plate was controlled by simply rotating the J-plate itself. Various measured states from the laser, displayed on a generalized OAM sphere are shown in Fig. 9(a2). The transition patterns from one to the other allow visualization of lasing across vastly differing OAM values as superpositions with two concentric rings. Then, in a digital laser for on-demand intracavity selective excitation of second-harmonic higher-order modes, an SLM used for structured beam generation also acted as an end mirror of the laser resonator,[147] as shown in Fig. 9(b1). After SHG modes passed through the nonlinear KTP crystal, it was found that the near-field spatial intensity profiles of the SHG LG modes in Fig. 9(b3) are similar to the intensity profile of the fundamental LG pump modes in Fig. 9(b2). But at the far field, the spatial intensity profiles of the SHG LG modes in Fig. 9(b4) are different from the fundamental pump modes because there is an added central intensity maximum, while in another intracavity SHG generation laser, the spatial distributions of the SHG beams are almost the same as that of the pump beams,[148] as shown in Figs. 9(c2)–9(c3). For some SHG patterns, the topological charge was found to have doubled, as shown in Fig. 9(c4). The generation of high-order modes was obtained by the off-axis displacement of the output coupling mirror and the SHG process was through the intracavity BBO crystal, as shown in Fig. 9(c1). In addition, investigations on the SHG structured laser beams in the TML states have been carried out.[149] Through a sandwich-like microchip laser composed of Nd:YAG, Cr:YAG, and LTO crystals in Fig. 9(d1), complex and diverse structured beams in TML states and their SHG beams were generated by altering the pumping parameters. As shown in Figs. 9(d2)–9(d3), a set of TML beams composed of the HG and LG modes and their SHG beams were obtained experimentally and agreed well with the theoretical simulation model as follows:

$$\begin{aligned} E_{\mathrm{SHG}}(r,\varphi) &\propto [XG_{m1,n1}(r,\varphi) + e^{i\phi} XG_{m2,n2}(r,\varphi)] \\ &\quad \times [XG_{m1,n1}(r,\varphi) + e^{i\phi} XG_{m2,n2}(r,\varphi)] \\ &= XG_{m1,n1}^2(r,\varphi) + 2e^{i\phi} XG_{m1,n1}(r,\varphi) XG_{m2,n2}(r,\varphi) \\ &\quad + e^{i2\phi} XG_{m2,n2}^2(r,\varphi). \end{aligned} \tag{24}$$

The complex transverse patterns in the TML states were composed of different basic modes with different weight coefficients and different locking phases, which makes the spatial information of the fundamental frequency mode and its SHG beam quite abundant.

In summary, combining the nonlinear transformation with the study of structured laser beams, the beam patterns are endowed with richer spatial information characteristics. For external cavity nonlinear process of structured laser beams, the law of OAM conservation during nonlinear interactions of LG beams was found. For SHG and SFG modes of the special LG beams, the propagation of the output beam patterns from near-field to far-field shows varying spatial characteristics. For intracavity nonlinear processes of structured laser beams, much more complex and diverse beam patterns could be obtained. In general, as a new research field of structured laser beams, the nonlinear process of beam shaping can be widely used in 3D printing, optical trapping, and free-space optical communication. In addition, as reviewed in Secs. 3 and 4, since there are many techniques for generating spatial and spatiotemporal structured beams. By applying nonlinear transformation technology, it is expected that the future of structured laser beams will have broader development prospects.

6 Conclusions and Perspectives

This paper is dedicated to reviewing the evolution of the spatial patterns of structured laser beams, covering the spontaneous organization of patterns described by relative equations and the advancements of on-demand transformations of laser patterns. Taking the spatial pattern as the core, we first reviewed the theoretical basis of laser transverse mode formation and emphasized its electromagnetic field properties and the dynamic mechanisms described by the related equations. Then, we analyzed the latest developments in the spatial characteristics of structured laser beam patterns through eigenmode superposition theory. With the coherent and incoherent superposition of laser eigenmodes, complex and diverse spatial patterns of structured laser beams can be generated. These studies on the spatial characteristics of structured laser beams are often conducted under the premise of a single longitudinal mode. However, if multiple longitudinal modes are involved, the time dimension needs to be accounted for. Therefore, we later reviewed the research on spatiotemporal structured laser beams, including direct generation by spatiotemporal mode-locking effect in fiber lasers and indirect regulation through the pulse shaper based on SLM. Moreover, it was found that the structured laser patterns could be endowed with richer spatial information characteristics through nonlinear conversion processes. We finally reviewed various nonlinear processes of structured laser patterns ranging

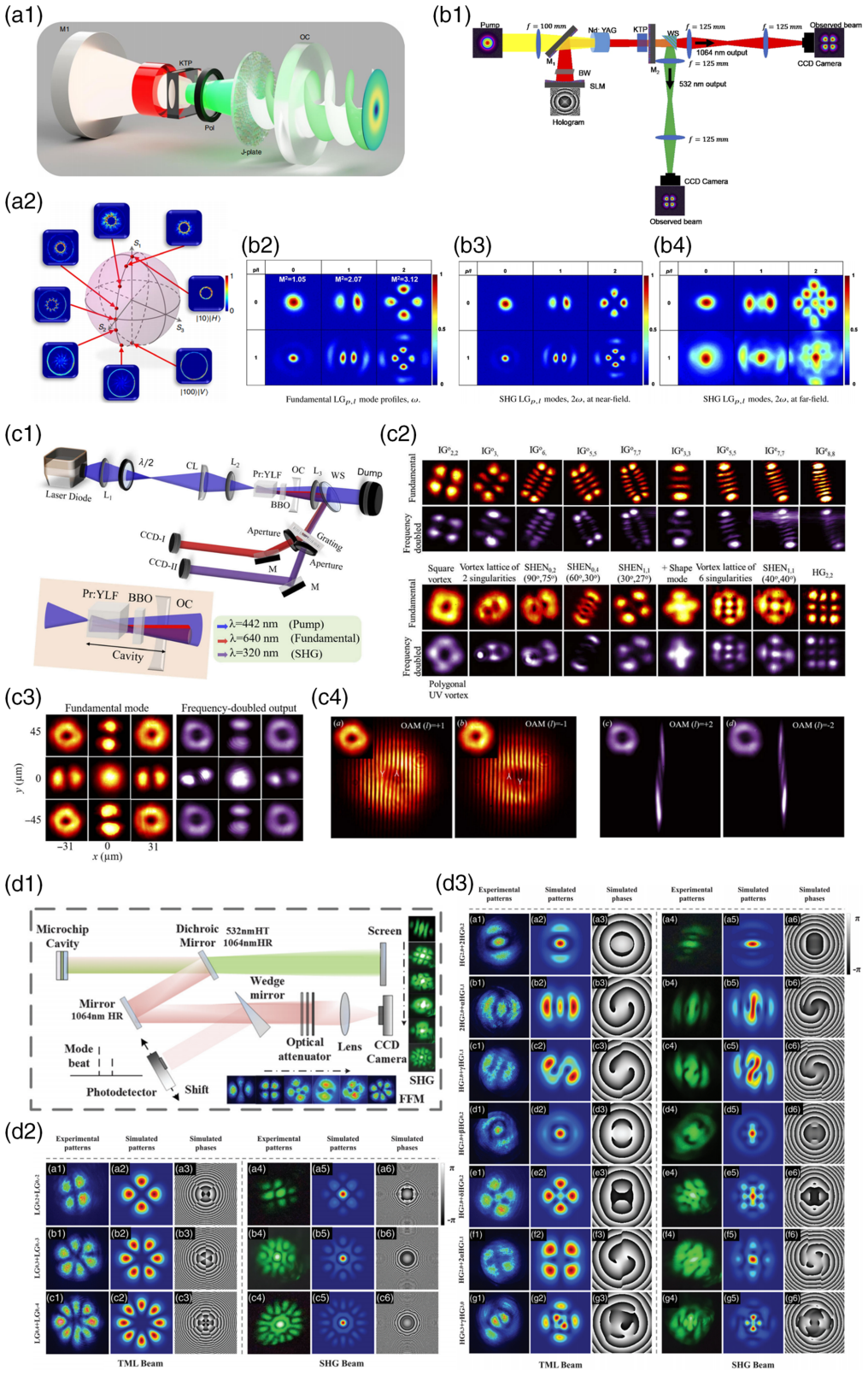

Fig. 9 Intracavity nonlinear process of structured laser beams. (a) Experimental setup and results to generate intracavity frequency-doubled LG beams. Adapted from Ref. 146. (b) Experimental setup and results showing near- and far-field SHG LG beams. Adapted from Ref. 147. (c) Experimental setup and results showing SHG optical vortices. Adapted from Ref. 148. (d) Experimental setup and results showing SHG modes of structured laser beams in the TML states. Adapted from Ref. 149.

from external cavity modulations to intracavity transformation comprehensively. Looking back over these 10 years, we can see how much our research and understanding of laser spatial features have advanced from classical to quantum,[213] especially since the discovery of OAM in the 1990s. However, the study of structured laser beams may just be in its early stages. We still have many unexplored novel phenomena and theories. There is potential for new and improved applications based on these spatial and temporal properties of laser modes, which could facilitate further research on novel laser spatial structures.

Acknowledgments

The authors declare no conflict of interest.

References

1. T. H. Maiman, "Stimulated optical radiation in ruby," *Nature* **187**, 493–494 (1960).
2. Y. S. Kivshar et al., "Dynamics of optical vortex solitons," *Opt. Commun.* **152**(1–3), 198–206 (1998).
3. F. Encinas-Sanz, S. Melle, and O. G. Calderón, "Time-resolved dynamics of two-dimensional transverse patterns in broad area lasers," *Phys. Rev. Lett.* **93**(21), 213904 (2004).
4. P. Ryczkowski et al., "Real-time full-field characterization of transient dissipative soliton dynamics in a mode-locked laser," *Nat. Photonics* **12**(4), 221–227 (2018).
5. A. Giesen and J. Speiser, "Fifteen years of work on thin-disk lasers: results and scaling laws," *IEEE J. Sel. Top. Quantum Electron.* **13**(3), 598–609 (2007).
6. H. Daido, M. Nishiuchi, and A. S. Pirozhkov, "Review of laser-driven ion sources and their applications," *Rep. Prog. Phys.* **75**(5), 56401 (2012).
7. M. N. Zervas and C. A. Codemard, "High power fiber lasers: a review," *IEEE J. Sel. Top. Quantum Electron.* **20**(5), 219–241 (2014).
8. Y. Yang et al., "Whispering-gallery mode hexagonal micro-/nanocavity lasers [invited]," *Photonics Res.* **7**(05), 594–131 (2019).
9. C. Lecompte et al., "Laser temporal-coherence effects on multiphoton ionization processes," *Phys. Rev. A* **11**(3), 1009–1015 (1975).
10. M. Skowronek, "Investigation of laser temporal pulse duration on Rayleigh scattering," *Phys. Rev. A* **27**(6), 3349–3350 (1983).
11. V. Hohreiter, J. E. Carranza, and D. W. Hahn, "Temporal analysis of laser-induced plasma properties as related to laser-induced breakdown spectroscopy," *Spectrochim. Acta Part B At. Spectrosc.* **59**(3), 327–333 (2004).
12. O. Lundh et al., "Few femtosecond, few kiloampere electron bunch produced by a laser–plasma accelerator," *Nat. Phys.* **7**(3), 219–222 (2011).
13. T. Herr et al., "Temporal solitons in optical microresonators," *Nat. Photonics* **8**(2), 145–152 (2014).
14. P. K. Maroju et al., "Attosecond pulse shaping using a seeded free-electron laser," *Nature* **578**(7795), 386–391 (2020).
15. S. P. Obenschain et al., "Laser-target interaction with induced spatial incoherence," *Phys. Rev. Lett.* **56**(26), 2807–2810 (1986).
16. A. M. Yao and M. J. Padgett, "Orbital angular momentum: origins, behavior and applications," *Adv. Opt. Photonics* **3**(2), 161 (2011).
17. Y. Shen et al., "Creation and control of high-dimensional multipartite classically entangled light," *Light Sci Appl* **10**(1), 50 (2021).
18. C. Rosales-Guzmán, B. Ndagano, and A. Forbes, "A review of complex vector light fields and their applications," *J. Opt.* **20**(12), 123001 (2018).
19. F. Ferdous et al., "Spectral line-by-line pulse shaping of on-chip microresonator frequency combs," *Nat. Photonics* **5**(12), 770–776 (2011).
20. A. Hugi et al., "Mid-infrared frequency comb based on a quantum cascade laser," *Nature* **492**(7428), 229–233 (2012).
21. G. Herink et al., "Resolving the build-up of femtosecond mode-locking with single-shot spectroscopy at 90 MHz frame rate," *Nat. Photonics* **10**(5), 321–326 (2016).
22. W. Liang et al., "High spectral purity Kerr frequency comb radio frequency photonic oscillator," *Nat. Commun.* **6**, 7957 (2015).
23. C. R. Petersen et al., "Mid-infrared supercontinuum covering the $1.4-13.3\ \mu$m molecular fingerprint region using ultra-high NA chalcogenide step-index fibre," *Nat. Photonics* **8**(11), 830–834 (2014).
24. J. Geng, "Structured-light 3D surface imaging: a tutorial," *Adv. Opt. Photonics* **3**(2), 128–160 (2011).
25. C. Maurer et al., "What spatial light modulators can do for optical microscopy," *Laser Photonics Rev.* **5**(1), 81–101 (2011).
26. R. Heintzmann and M. Gustafsson, "Subdiffraction resolution in continuous samples," *Nat. Photonics* **3**(7), 362–364 (2009).
27. J. Huisken et al. "Optical sectioning deep inside live embryos by selective plane illumination microscopy," *Science* **305**(5686), 1007–1009 (2004).
28. A. Belmonte and J. P. Torres, "Optical Doppler shift with structured light," *Opt. Lett.* **36**(22), 4437–4439 (2011).
29. C. Rosales-Guzmán et al., "Experimental detection of transverse particle movement with structured light," *Sci. Rep.* **3**, 2815 (2013).
30. B. Aniceto et al., "A measure of flow vorticity with helical beams of light," *Optica* **2**(11), 1002–1005 (2015).
31. J. Wang et al., "Terabit free-space data transmission employing orbital angular momentum multiplexing," *Nat. Photonics* **6**(7), 488–496 (2012).
32. J. Wang, "Advances in communications using optical vortices," *Photonics Res.* **4**(5), B14–B28 (2016).
33. L. Gong et al., "Optical orbital-angular-momentum-multiplexed data transmission under high scattering," *Light Sci. Appl.* **8**(1), 27 (2019).
34. M. Padgett and R. Bowman, "Tweezers with a twist," *Nat. Photonics* **5**(6), 343–348 (2011).
35. C. Kuo and S. Chu, "Numerical study of the properties of optical vortex array laser tweezers," *Opt. Express* **21**(22), 26418–26431 (2013).
36. W. Mike et al., "Advanced optical trapping by complex beam shaping," *Laser Photonics Rev.* **7**(6), 839–854 (2013).
37. X. L. Wang et al., "Quantum teleportation of multiple degrees of freedom of a single photon," *Nature* **518**(7540), 516 (2015).
38. B. Ndagano et al., "Creation and detection of vector vortex modes for classical and quantum communication," *J. Lightwave Technol.* **36**(2), 292–301 (2018).
39. A. Sit et al., "High-dimensional intracity quantum cryptography with structured photons," *Optica* **4**(9), 1006 (2017).
40. A. Forbes, "Structured light from lasers," *Laser Photonics Rev.* **13**(11), 1900140 (2019).
41. Y. F. Chen et al., "Laser transverse modes of spherical resonators: a review [Invited]," *Chin. Opt. Lett.* **18**(9), 91404 (2020).
42. A. Forbes, M. D. Oliveira, and M. R. Dennis, "Structured light," *Nat. Photonics* **15**, 253–262 (2021).
43. M. V. Berry and M. R. Dennis, "Roadmap on structured light," *J. Opt.* **2**(19), 013001 (2017).
44. O. V. Angelsky et al., "Structured light: ideas and concepts," *Front. Phys.* **8**, 114 (2020).
45. J. Wang et al., "Generation and detection of structured light," *Front. Phys.* **9**, 688284 (2021).
46. C. D. E. Otte, "Optical trapping gets structure: structured light for advanced optical manipulation," *Appl. Phys. Rev.* **7**(4), 41308 (2020).

47. Y. Yang et al., "Optical trapping with structured light," *Adv. Photonics* **3**(3), 34001 (2021).
48. M. A. Cox et al., "Structured light in turbulence," *IEEE J. Sel. Top. Quantum Electron.* **2**(27), 1–21 (2020).
49. L. Feng et al. "A review of tunable orbital angular momentum modes in fiber: principle and generation," *Appl. Sci.* **9**(12), 2408 (2019).
50. Y. Shen et al., "Optical vortices 30 years on: OAM manipulation from topological charge to multiple singularities," *Light Sci. Appl.* **8**, 90 (2019).
51. J. Ni et al, "Multidimensional phase singularities in nanophotonics," *Science* **374**, 418 (2021).
52. C. He, Y. Shen, and A. Forbes, "Towards higher-dimensional structured light," *Light Sci. Appl.* **11**, 205 (2022).
53. A. H. Dorrah and F. Capasso, "Tunable structured light with flat optics," *Science* **376**, 367 (2022).
54. W. T. Buono and A. Forbes, "Nonlinear optics with structured light," *Opto-Electron Adv.* **5**, 210174 (2022).
55. N. G. Basov, V. N. Morozov, and A. N. Oraevskiĭ, "Nonlinear mode interaction in lasers," *Sov. J. Exp. Theor. Phys.* **22**, 895–904 (1966).
56. A. F. Suchkov, "Effect of inhomogeneities on the operation regime of solid-state lasers," *Sov. J. Exp. Theor. Phys.* **49**, 1495–1903 (1966).
57. R. Graham and H. Haken, "Laserlight–first example of a second-order phase transition far away from thermal equilibrium," *Ztschr. Phys.* **237**(1), 31–46 (1970).
58. V. E. Zakharov and A. B. Shabat, "Exact theory of two-dimensional self-focusing and one-dimensional self-modulation of waves in nonlinear media," *J. Exp. Theor. Phys.* **34**, 62–69 (1972).
59. M. V. Berry, J. F. Nye, and F. J. Wright, "The elliptic umbilic diffraction catastrophe," *Philos. Trans. R. Soc. A* **291**, 453–484 (1979).
60. K. I. Kubodera and K. Otsuka, "Single-transverse-mode $LiNdP_4O_{12}$ slab waveguide laser," *J. Appl. Phys.* **50**(2), 653–659 (1979).
61. N. B. Baranova et al., "Dislocations of the wavefront of a speckle-inhomogeneous field (theory and experiment)," *JETP Lett.* **33**, 195 (1981).
62. L. A. Lugiato, L. M. Narducci, and C. Oldano, "Cooperative frequency locking and stationary spatial structures in lasers," *J. Opt. Soc. Am. B* **5**(5), 879 (1988).
63. P. Coullet, L. Gil, and F. Rocca, "Optical vortices," *Opt. Commun.* **73**(5), 403–408 (1989).
64. J. V. Moloney and A. C. Newell, "Nonlinear optics," *Physica D* **44**(1), 1–37 (1990).
65. L. A. Lugiato et al., "Instabilities and spatial complexity in a laser," *J. Opt. Soc. Am. B* **7**(6), 1019–1033 (1990).
66. Q. S. Yang et al, "Global stability and oscillation properties of a two-level model for a class-B laser with feedback," *Opt. Commun.* **138**(4–6), 325–329 (1997).
67. G. L. Oppo, G. D Alessandro, and W. J. Firth, "Spatiotemporal instabilities of lasers in models reduced via center manifold techniques," *Phys. Rev. A* **44**(7), 4712–4720 (1991).
68. F. T. Arecchi et al., "Deterministic chaos in laser with injected signal," *Opt. Commun.* **51**(5), 308–314 (1984).
69. W. Greiner, "Classical electrodynamics," *Phys. Today* **52**(10), 78 (1999).
70. C. Coste, "Nonlinear Schrödinger equation and superfluid hydrodynamics," *Eur. Phys. J. B* **2** 245–253 (1998).
71. E. A. Arecchi, "Pattern formation and competition in nonlinear optics," *Phys. Rep.* **318**(1-6), 1–83 (1999).
72. Y. Castin and K. Mo Lmer, "Maxwell–Bloch equations: a unified view of nonlinear optics and nonlinear atom optics," *Phys. Rev. A* **51**(5), R3426 (1995).
73. K. Staliunas, "Laser Ginzburg–Landau equation and laser hydrodynamics," *Phys. Rev. A* **48**(2), 1573 (1993).
74. K. Staliunas and C. O. Weiss, "Tilted and standing waves and vortex lattices in class-A lasers," *Physica D* **81**(1–2), 79–93 (1995).
75. J. Swift and P. C. Hohenberg, "Hydrodynamic fluctuations at the convective instability," *Phys. Rev. A* **15**(1), 319–328 (1977).
76. K. Staliunas and C. O. Weiss, "Nonstationary vortex lattices in large-aperture class B lasers," *J. Opt. Soc. Am. B* **12**(6), 1142 (1995).
77. G. Huyet et al., "Spatiotemporal dynamics of lasers with a large Fresnel number," *Phys. Rev. Lett.* **75**(22), 4027–4030 (1995).
78. Y. Kuramoto and T. Yamada, "Pattern formation in oscillatory chemical reactions," *Prog. Theor. Phys.* **55**, 356 (1976).
79. R. Lefever et al., "Phase dynamics of transverse diffraction patterns in the laser," *Phys. Lett. A* **135**(4–5), 254–258 (1989).
80. N. A. Kudryashov, "Exact solutions of the generalized Kuramoto–Sivashinsky equation," *Phys. Lett. A* **147**(5–6), 287–291 (1990).
81. B. J. Gluckman et al., "Time averaging of chaotic spatiotemporal wave patterns," *Phys. Rev. Lett.* **71**(13), 2034 (1993).
82. L. A. Lugiato, "Nonlinear optical structures, patterns and chaos," *Chaos Soliton. Fract.* **4**(8/9), 1251–1258 (1994).
83. P. Mandel and M. Tlidi, "Transverse dynamics in cavity nonlinear optics," *J. Opt. B* **6**(9), R60 (2004).
84. Y. F. Chen and Y. P. Lan, "Formation of optical vortex lattices in solid-state microchip lasers: spontaneous transverse mode locking," *Phys. Rev. A* **64**(6), 63807 (2001).
85. Y. F. Chen and Y. P. Lan, "Transverse pattern formation of optical vortices in a microchip laser with a large Fresnel number," *Phys. Rev. A* **65**(1), 13802 (2001).
86. G. D'Alessandro et al., "Average patterns and coherent phenomena in wide aperture lasers," *Phys. Rev. E* **69**(6 Pt 2), 66212 (2004).
87. J. Scheuer and M. Orenstein, "Optical vortices crystals: spontaneous generation in nonlinear semiconductor microcavities," *Science* **285**(5425), 230–233 (1999).
88. K. Otsuka and S. Chu, "Generation of vortex array beams from a thin-slice solid-state laser with shaped wide-aperture laser-diode pumping," *Opt. Lett.* **34**(1), 10–12 (2009).
89. Y. Shen et al., "Vortex lattices with transverse-mode-locking states switching in a large-aperture off-axis-pumped solid-state laser," *J. Opt. Soc. Am. B* **35**(12), 2940 (2018).
90. L. Allen et al., "Orbital angular momentum of light and transformation of Laguerre Gaussian laser modes," *Phys. Rev. A* **45**(11), 8185–8189 (1992).
91. M. A. Bandres and J. C. Gutiérrez-Vega, "Ince–Gaussian modes of the paraxial wave equation and stable resonators," *J. Opt. Soc. Am. A:* **21**(5), 873–880 (2004).
92. J. Durnin, J. J. Miceli, Jr., and J. H. Eberly, "Diffraction-free beams," *Phys. Rev. Lett.* **58**(15), 1499–1501 (1987).
93. V. Garcés-Chávez et al., "Observation of the transfer of the local angular momentum density of a multiringed light beam to an optically trapped particle," *Phys. Rev. Lett.* **91**(9), 93602 (2003).
94. R. P. Macdonald et al. "Interboard optical data distribution by Bessel beam shadowing," *Opt. Commun.* **122**(4–6), 169–177 (1996).
95. Y. Li et al., "Classically-entangled Ince–Gaussian modes," *Appl. Phys. Lett.* **22**(116), 221105 (2020).
96. J. C. Gutierrez-Vega and M. A. Bandres, "Helmholtz–Gauss waves," *J. Opt. Soc. Am. A:* **22**(2), 289–298 (2005).
97. P. W. Smith, "Simultaneous phase-locking of longitudinal and transverse laser modes," *Appl. Phys. Lett.* **13**(7), 235–237 (1968).
98. D. H. Auston, "Forced and spontaneous phase locking of the transverse modes of a He–Ne laser," *IEEE J. Quantum Electron.* **4**(7), 471–473 (1968).
99. Z. Zhang and C. Zhao, "Spontaneous phase and frequency locking of transverse modes in different orders," *Phys. Rev. Appl* **13**(2), 24010 (2020).
100. S. Mahler et al., "Improved phase locking of laser arrays with nonlinear coupling," *Phys. Rev. Lett.* **124**, 133901 (2020).

101. A. N. K. Reddy et al., "Phase locking of lasers with Gaussian coupling," *Opt. Express* **30**(2), 1114–1129 (2022).
102. M. Brambilla et al, "Transverse laser patterns. I. Phase singularity crystals," *Phys. Rev. A* **43**(9), 5090 (1991).
103. L. G. Wright, D. N. Christodoulides, and F. W. Wise, "Spatiotemporal mode-locking in multimode fiber lasers," *Science* **358**(6359), 94–97 (2017).
104. H. Qin et al., "Observation of soliton molecules in a spatiotemporal mode-locked multimode fiber laser," *Opt. Lett.* **43**(9), 1982–1985 (2018).
105. Y. Ding et al., "Multiple-soliton in spatiotemporal mode-locked multimode fiber lasers," *Opt. Express* **27**(8), 11435 (2019).
106. T. Mayteevarunyoo, B. A. Malomed, and D. V. Skryabin, "Spatiotemporal dissipative solitons and vortices in a multi-transverse-mode fiber laser," *Opt. Express* **27**(26), 37364 (2019).
107. L. G. Wright et al., "Mechanisms of spatiotemporal mode-locking," *Nat. Phys.* **16**(5), 565–570 (2020).
108. M. Bagci and J. N. Kutz, "Spatiotemporal mode locking in quadratic nonlinear media," *Phys. Rev. E* **102**(2-1), 22205 (2020).
109. X. Lin et al., "All few-mode fiber spatiotemporal mode-locked figure-eight laser," *J. Lightwave Technol.* **39**(17), 5611–5616 (2021).
110. Y. Ding et al., "Spatiotemporal mode-locking in lasers with large modal dispersion," *Phys. Rev. Lett.* **126**(9), 93901 (2021).
111. F. Frei, A. Galler, and T. Feurer, "Space-time coupling in femtosecond pulse shaping and its effects on coherent control," *J. Chem. Phys.* **130**(3), 34302 (2009).
112. G. Pariente et al., "Space-time characterization of ultra-intense femtosecond laser beams," *Nat. Photonics* **10**(8), 547–553 (2016).
113. Y. Wang et al., "High-power mode-locked 2 μm multimode fiber laser," *Laser Phys. Lett.* **15**(8), 85101 (2018).
114. M. Kowalczyk et al., "Ultrabroadband wavelength-swept source based on total mode-locking of an $Yb:CaF_2$ laser," *Photonics Res.* **7**(2), 182 (2019).
115. K. Krupa et al., "Multimode nonlinear fiber optics, a spatiotemporal avenue," *APL Photonics* **4**(11), 110901 (2019).
116. W. H. Renninger, A. Chong, and F. W. Wise, "Pulse shaping and evolution in normal-dispersion mode-locked fiber lasers," *IEEE J. Sel. Top. Quantum. Electron.* **18**, 389–398 (2012).
117. A. Chong, L. G. Wright, and F. W. Wise, "Ultrafast fiber lasers based on self-similar pulse evolution: a review of current progress," *Rep. Prog. Phys.* **78**, 113901 (2015).
118. A. Chong et al., "Generation of spatiotemporal optical vortices with controllable transverse orbital angular momentum," *Nat. Photonics* **14**(6), 350–354 (2020).
119. A. Mirando et al., "Generation of spatiotemporal optical vortices with partial temporal coherence," *Opt. Express* **29**(19), 30426 (2021).
120. Q. Cao et al., "Sculpturing spatiotemporal wavepackets with chirped pulses," *Photonics Res.* **9**(11), 2261 (2021).
121. H. E. Kondakci and A. F. Abouraddy, "Diffraction-free space-time light sheets," *Nat. Photonics* **11**(11), 733–740 (2017).
122. M. Dallaire, N. McCarthy, and M. Piché, "Spatiotemporal Bessel beams: theory and experiments," *Opt. Express* **17**(20), 18148–18164 (2009).
123. B. Sun et al., "Four-dimensional light shaping: manipulating ultrafast spatiotemporal foci in space and time," *Light Sci. Appl.* **7**(1), 17117 (2018).
124. H. E. Kondakci and A. F. Abouraddy, "Diffraction-free pulsed optical beams via space-time correlations," *Opt. Express* **24**(25), 28659 (2016).
125. M. Mounaix et al., "Time reversed optical waves by arbitrary vector spatiotemporal field generation," *Nat. Commun.* **11**, 5813 (2020).
126. C. Wan et al., "Toroidal vortices of light," *Nat. Photonics* **16**, 519–522 (2022).
127. A. Beržanskis et al., "Sum-frequency mixing of optical vortices in nonlinear crystals," *Opt. Commun.* **150**(1), 372–380 (1998).
128. Y. Li et al., "Sum frequency generation with two orbital angular momentum carrying laser beams," *J. Opt. Soc. Am. B* **32**(3), 407 (2015).
129. Y. Li et al., "Dynamic mode evolution and phase transition of twisted light in nonlinear process," *J. Mod. Opt.* **63**(21), 2271–2278 (2016).
130. D. G. Pires et al., "Mixing Ince–Gaussian modes through sum-frequency generation," *J. Opt. Soc. Am. B* **37**(10), 2815 (2020).
131. K. Dholakia et al., "Second-harmonic generation and the orbital angular momentum of light," *Phys. Rev. A* **54**(5), R3742–R3745 (1996).
132. J. Courtial et al., "Second-harmonic generation and the conservation of orbital angular momentum with high-order Laguerre–Gaussian modes," *Phys. Rev. A* **56**(5), 4193–4196 (1997).
133. H. Yu et al., "Generation of crystal-structure transverse patterns via a self-frequency-doubling laser," *Sci. Rep.* **3**, 1085 (2013).
134. S. Li et al., "Managing orbital angular momentum in second-harmonic generation," *Phys. Rev. A* **88**(3), 035801 (2013).
135. W. T. Buono et al., "Arbitrary orbital angular momentum addition in second harmonic generation," *New J. Phys.* **16**(9), 93041 (2014).
136. Z. Zhou et al., "Orbital angular momentum light frequency conversion and interference with quasi-phase matching crystals," *Opt. Express* **22**(17), 20298 (2014).
137. L. J. Pereira et al., "Orbital-angular-momentum mixing in type-II second-harmonic generation," *Phys. Rev. A* **96**(5), 053856 (2017).
138. Y. Tang et al., "Harmonic spin-orbit angular momentum cascade in nonlinear optical crystals," *Nat. Photonics* **14**(11), 658–662 (2020).
139. D. G. Pires et al., "Optical mode conversion through nonlinear two-wave mixing," *Phys. Rev. A* **100**(4) (2019).
140. D. G. Pires et al., "Higher radial orders of Laguerre–Gaussian beams in nonlinear wave mixing processes," *J. Opt. Soc. Am. B* **37**(5), 1328 (2020).
141. D. S. Ding et al., "Linear up-conversion of orbital angular momentum," *Opt. Lett.* **37**(15), 3270–3272 (2012).
142. G. Walker, A. S. Arnold, and S. Franke-Arnold, "Trans-spectral orbital angular momentum transfer via four-wave mixing in Rb vapor," *Phys. Rev. Lett.* **108**(24), 243601 (2012).
143. H. Yang et al., "Parametric upconversion of Ince–Gaussian modes," *Opt. Lett.* **45**(11), 3034–3037 (2020).
144. X. Y. Z. Xiong et al., "Mixing of spin and orbital angular momenta via second-harmonic generation in plasmonic and dielectric chiral nanostructures," *Phys. Rev. B* **95**(16), 165432 (2017).
145. H. Wu et al., "Radial modal transitions of Laguerre–Gauss modes during parametric up-conversion: towards the full-field selection rule of spatial modes," *Phys. Rev. A* **101**(6), 063805 (2020).
146. H. Sroor et al., "High-purity orbital angular momentum states from a visible metasurface laser," *Nat. Photonics* **14**(8), 498–503 (2020).
147. T. Bell, M. Kgomo, and S. Ngcobo, "Digital laser for on-demand intracavity selective excitation of second harmonic higher-order modes," *Opt. Express* **28**(11), 16907 (2020).
148. A. Srinivasa Rao, K. Miamoto, and T. Omatsu, "Ultraviolet intracavity frequency-doubled $Pr^{3+}:LiYF_4$ orbital Poincaré laser," *Opt. Express* **28**(25), 37397 (2020).
149. Z. Zhang et al., "Second harmonic generation of laser beams in transverse mode locking states," *Adv. Photonics* **2**(4), 026002 (2022).
150. M. C. Cross and P. C. Hohenberg, "Pattern formation outside of equilibrium," *Rev. Mod. Phys.* **65**(3), 851–1112 (1993).
151. M. Saffman, "Optical pattern formation," *Adv. At. Mol. Opt. Phys.* **40**(8), 229–306 (1998).
152. J. Joly, G. Metivier, and J. Rauch, "Transparent nonlinear geometric optics and Maxwell–Bloch equations," *J. Differ. Equ.* **166**, 175–250 (2000).

153. Y. F. Chen and Y. P. Lan, "Dynamics of the Laguerre Gaussian $TEM_{0,l}$ mode in a solid-state laser," *Phys. Rev. A* **6**(63), 63807 (2001).
154. E. N. Lorenz, "Deterministic nonperiodic flow," *J. Atmos. Sci.* **20**, 130–141 (1963).
155. N. B. Abraham and W. J. Firth, "Overview of transverse effects in nonlinear-optical systems," *J. Opt. Soc. Am. B* **7**(6), 951 (1990).
156. P. Coullet, C. Riera, and C. Tresser, "Stable static localized structures in one dimension," *Phys. Rev. Lett.* **84**(14), 3069 (2000).
157. K. I. Maruno, A. Ankiewicz, and N. Akhmediev, "Exact soliton solutions of the one-dimensional complex Swift–Hohenberg equation," *Physica D* **176**(1), 44–66 (2003).
158. B. J. Tepper, "Consequences of abusive supervision," *Acad. Manage. J.* **43**(2), 178–190 (2000).
159. Y. F. Chen and Y. P. Lan, "Dynamics of helical-wave emission in a fiber-coupled diode end-pumped solid-state laser," *Appl. Phys. B* **73**(1), 11–14 (2001).
160. M. A. Bandres, J. C. Gutiérrez-Vega, and S. Chávez-Cerda, "Parabolic nondiffracting optical wave fields," *Opt. Lett.* **29**(1), 44 (2004).
161. B. Zhao et al., "Parabolic-accelerating vector waves," *Nanophotonics* **11**(4), 681–688 (2022).
162. H. Kogelnik and T. Li, "Laser beams and resonators," *Appl. Opt.* **5**(10), 1550–1567 (1966).
163. Z. Wan et al., "Quadrant-separable multi-singularity vortices manipulation by coherent superposed mode with spatial-energy mismatch," *Opt. Express* **26**(26), 34940 (2018).
164. M. A. Bandres and J. C. Gutiérrez-Vega, "Ince–Gaussian beams," *Opt. Lett.* **29**(2), 144 (2004).
165. S. C. Chu and K. Otsuka, "Numerical study for selective excitation of Ince–Gaussian modes in end-pumped solid-state lasers," *Opt. Express* **15**(25), 16506–16519 (2008).
166. N. Barré, M. Romanelli, and M. Brunel, "Role of cavity degeneracy for high-order mode excitation in end-pumped solid-state lasers," *Opt. Lett.* **39**(4), 1022–1025 (2014).
167. D. Mcgloin and K. Dholakia, "Bessel beams: diffraction in a new light," *Contemp. Phys.* **46**(1), 15–28 (2005).
168. V. Garcés-Chávez et al., "Simultaneous micromanipulation in multiple planes using a self-reconstructing light beam," *Nature* **419**(6903), 145–147 (2002).
169. J. C. Gutiérrez-Vega et al., "Alternative formulation for invariant optical fields: Mathieu beams," *Opt. Lett.* **25**(20), 1493–1495 (2000).
170. J. C. Gutiérrez-Vega et al., "Experimental demonstration of optical Mathieu beams," *Opt. Commun.* **195**(1–4), 35–40 (2001).
171. S. Chávez-Cerda et al., "Holographic generation and orbital angular momentum of high-order Mathieu beams," *J. Opt. Soc. Am. B* **4**(2), S52–S57 (2002).
172. G. A. Siviloglou and D. N. Christodoulides, "Accelerating finite energy Airy beams," *Opt. Lett.* **32**(8), 979–981 (2007).
173. G. A. Siviloglou et al., "Observation of accelerating Airy beams," *Phys. Rev. Lett.* **4**, S52 (2007).
174. Y. Shen et al., "SU(2) Poincaré sphere: a generalized representation for multidimensional structured light," *Phys. Rev. A* **102**(3), 031501 (2020).
175. E. Abramochkin and T. Alieva, "Closed-form expression for mutual intensity evolution of Hermite–Laguerre–Gaussian Schell-model beams," *Opt. Lett.* **42**(19), 4032 (2017).
176. W. N. Plick et al., "Quantum orbital angular momentum of elliptically symmetric light," *Phys. Rev. A* **87**, 033806 (2013).
177. Y. Shen et al., "Periodic-trajectory-controlled, coherent-state-phase-switched, and wavelength-tunable SU(2) geometric modes in a frequency-degenerate resonator," *Appl. Opt.* **57**(32), 9543 (2018).
178. Y. Shen et al., "Hybrid topological evolution of multi-singularity vortex beams: generalized nature for helical-Ince–Gaussian and Hermite–Laguerre-Gaussian modes," *J. Opt. Soc. Am. A:* **36**, 578 (2019).
179. M. J. Padgett and J. Courtial, "Poincaré-sphere equivalent for light beams containing orbital angular momentum," *Opt. Lett.* **24**(7), 430–432 (1999).
180. E. Abramochkin and V. Volostnikov, "Beam transformations and nontransformed beams," *Opt. Commun.* **83**(1–2), 123–135 (1991).
181. M. W. Beijersbergen et al., "Astigmatic laser mode converters and transfer of orbital angular momentum," *Opt. Commun.* **96**(1–3), 123–132 (1993).
182. E. G. Abramochkin and V. G. Volostnikov, "Generalized Gaussian beams," *J. Opt. A* **6**(5), S157 (2004).
183. E. G. Abramochkin and V. G. Volostnikov, "Generalized Hermite–Laguerre–Gauss beams," *Phys. Wave Phenom.* **18**(1), 14–22 (2010).
184. Y. Shen, X. Fu, and M. Gong, "Truncated triangular diffraction lattices and orbital-angular-momentum detection of vortex SU(2) geometric modes," *Opt. Express* **26**, 25545 (2018).
185. Y. Shen et al., "Structured ray-wave vector vortex beams in multiple degrees of freedom from a laser," *Optica* **7**(7), 820 (2020).
186. M. Woerdemann, C. Alpmann, and C. Denz, "Optical assembly of microparticles into highly ordered structures using Ince–Gaussian beams," *Appl. Phys. Lett.* **98**(11), 111101 (2011).
187. J. A. Davis et al., "Generation of helical Ince–Gaussian beams: beam-shaping with a liquid crystal display," *Proc. SPIE* **6290**, 62900R (2006).
188. J. B. Bentley et al., "Generation of helical Ince–Gaussian beams with a liquid-crystal display," *Opt. Lett.* **31**(5), 649–651 (2006).
189. S. M. Baumann et al., "Propagation dynamics of optical vortices due to Gouy phase," *Opt. Express* **17**(12), 9818–9827 (2009).
190. E. Louvergneaux et al., "Coupled longitudinal and transverse self-organization in lasers induced by transverse-mode locking," *Phys. Rev. A* **57**(6), 4899–4904 (1998).
191. Y. F. Chen, K. F. Huang, and Y. P. Lan, "Spontaneous transverse patterns in a microchip laser with a frequency-degenerate resonator," *Opt. Lett.* **28**(19), 1811–1813 (2003).
192. A. S. Rao et al., "Optical vortex lattice mode generation from a diode-pumped Pr^{3+}:$LiYF_4$ laser," *J. Opt.* **23**(7), 75502 (2021).
193. Y. Cao et al., "Transverse patterns and dual-frequency lasing in a low-noise nonplanar-ring orbital-angular-momentum oscillator," *Phys. Rev. Appl.* **13**(2), 024067 (2020).
194. X. Wang et al., "Investigation on the formation of laser transverse pattern possessing optical lattices," *Front. Phys.* **9**(1), 801916 (2022).
195. E. Louvergneaux et al., "Transverse mode competition in a CO_2 laser," *Phys. Rev. A* **53**(6), 4435 (1996).
196. R. Oron et al., "Laser mode discrimination with intra-cavity spiral phase elements," *Opt. Commun.* **169**(1–6), 115–121 (1999).
197. K. Sueda et al., "Laguerre–Gaussian beam generated with a multilevel spiral phase plate for high intensity laser pulses," *Opt. Express* **12**(15), 3548–3553 (2004).
198. W. M. Lee, X. C. Yuan, and W. C. Cheong, "Optical vortex beam shaping by use of highly efficient irregular spiral phase plates for optical micromanipulation," *Opt. Lett.* **29**(15), 1796–1798 (2004).
199. D. J. Kim and J. W. Kim, "High-power TEM00 and Laguerre–Gaussian mode generation in double resonator configuration," *Appl. Phys. B* **121**(3), 401–405 (2015).
200. D. J. Kim, J. I. Mackenzie, and J. W. Kim, "Adaptable beam profiles from a dual-cavity Nd:YAG laser," *Opt. Lett.* **41**(8), 1740–1743 (2016).
201. L. Marrucci, C. Manzo, and D. Paparo, "Optical spin-to-orbital angular momentum conversion in inhomogeneous anisotropic media," *Phys. Rev. Lett.* **96**(16), 163905 (2006).
202. L. Marrucci, "The q-plate and its future," *J. Nanophotonics* **7**(1), 078598 (2013).
203. B. Piccirillo et al., "Photon spin-to-orbital angular momentum conversion via an electrically tunable q-plate," *Appl. Phys. Lett.* **97**(24), 241104 (2010).

204. D. Naidoo et al., "Controlled generation of higher-order Poincaré sphere beams from a laser," *Nat. Photonics* **10**(5), 327–332 (2016).
205. R. R. Alfano, G. Milione, E. J. Galvez, and L. Shi, "A laser for complex spatial modes," *Nat. Photonics* **10**(5), 286–288 (2016).
206. S. Ngcobo et al., "A digital laser for on-demand laser modes," *Nat. Commun.* **4**, 2289 (2013).
207. L. Burger et al., "Implementation of a spatial light modulator for intracavity beam shaping," *J. Opt.* **17**(1), 15604 (2015).
208. A. Forbes, A. Dudley, and M. McLaren, "Creation and detection of optical modes with spatial light modulators," *Adv. Opt. Photonics* **8**(2), 200 (2016).
209. S. Scholes et al., "Structured light with digital micromirror devices: a guide to best practice," *Opt. Eng.* **59**(4), 041202 (2020).
210. C. W. Johnson et al., "Exact design of complex amplitude holograms for producing arbitrary scalar fields," *Opt. Express* **28**(12), 17334–17346 (2020).
211. C. Rosales-Guzmán et al., "Polarisation-insensitive generation of complex vector modes from a digital micromirror device," *Sci. Rep.* **10**(1), 10434 (2020).
212. P. Chen et al., "Liquid-crystal-mediated geometric phase: from transmissive to broadband reflective planar optics," *Adv. Mater.* **32**(27), 1903665 (2019).
213. Y. Shen and C. Rosales-Guzmán, "Nonseparable states of light: from quantum to classical," *Laser Photonics Rev.* **16**(7), 2100533 (2022).

Biographies of the authors are not available.